



저작자표시-비영리-변경금지 2.0 대한민국

이용자는 아래의 조건을 따르는 경우에 한하여 자유롭게

- 이 저작물을 복제, 배포, 전송, 전시, 공연 및 방송할 수 있습니다.

다음과 같은 조건을 따라야 합니다:



저작자표시. 귀하는 원저작자를 표시하여야 합니다.



비영리. 귀하는 이 저작물을 영리 목적으로 이용할 수 없습니다.



변경금지. 귀하는 이 저작물을 개작, 변형 또는 가공할 수 없습니다.

- 귀하는, 이 저작물의 재이용이나 배포의 경우, 이 저작물에 적용된 이용허락조건을 명확하게 나타내어야 합니다.
- 저작권자로부터 별도의 허가를 받으면 이러한 조건들은 적용되지 않습니다.

저작권법에 따른 이용자의 권리는 위의 내용에 의하여 영향을 받지 않습니다.

이것은 [이용허락규약\(Legal Code\)](#)을 이해하기 쉽게 요약한 것입니다.

[Disclaimer](#)

A THESIS FOR THE DEGREE OF MASTER OF SCIENCE

**Surface modification of hydroxyapatite with PLGA and
properties of PLGA/HA composites with different preparation methods**

**PLGA를 이용한 하이드록시아파타이트의 표면 개질 및
제조 방법에 따른 PLGA/HA 복합재의 물성 연구**

Jin-Uk Hwang

**PROGRAM IN ENVIRONMENTAL MATERIALS SCIENCE
GRADUATE SCHOOL
SEOUL NATIONAL UNIVERSITY**

August, 2019

A THESIS FOR THE DEGREE OF MASTER OF SCIENCE

**Surface modification of hydroxyapatite with PLGA and
properties of PLGA/HA composites with different preparation methods**

**PLGA를 이용한 하이드록시아파타이트의 표면 개질 및
제조 방법에 따른 PLGA/HA 복합재의 물성 연구**

Jin-Uk Hwang

Adviser : Hyun-Joong Kim

**PROGRAM IN ENVIRONMENTAL MATERIALS SCIENCE
GRADUATE SCHOOL
SEOUL NATIONAL UNIVERSITY**

August, 2019

**Surface modification of hydroxyapatite with PLGA and
properties of PLGA/HA composites with different preparation methods**

**PLGA를 이용한 하이드록시아파타이트의 표면 개질 및
제조 방법에 따른 PLGA/HA 복합재의 물성 연구**

지도교수: 김 현 중

이 논문을 농학석사학위 논문으로 제출함
2019 년 5 월

서울대학교 대학원
산림과학부 환경재료과학전공
황 진 욱

황진욱의 석사학위 논문을 인준함
2019 년 6 월

위 원 장 윤 혜 정 (인)

부위원장 김 현 중 (인)

위 원 오 정 권 (인)

Abstract

Surface modification of hydroxyapatite with PLGA and properties of PLGA/HA composites with different preparation methods

Jin-Uk Hwang

Program in Environmental Materials Science

The Graduate School

Seoul National University

In this study, poly(lactide-*co*-glycolide) (PLGA) polymer chains were directly grafted onto the surface hydroxyl groups of hydroxyapatite (HA) to observe the effects of HA surface modification on the interfacial adhesion, and thus the properties, of PLGA/PLGA-g-HA composites. Spectroscopic analysis indicated ester linkage formation at the HA surface, with the grafted polymer content of 10.032 wt%. Solid-state ¹H nuclear magnetic resonance spectra indicated that the amount of HA surface hydroxyl groups decreased by 3.125% after grafting. Molecular weight reduction was measured by gel permeation chromatography. X-ray diffraction patterns and scanning electron microscopy micrographs further verified successful grafting. After grafting, PLGA/PLGA-g-HA composites were prepared via three different preparation methods. The thermal, mechanical, and viscoelastic properties of the composites were determined by differential scanning calorimetry, tensile testing, and dynamic mechanical analysis, respectively. The results show that the preparation method has important effects on the properties of the final PLGA/PGA-g-HA composite.

Keywords: Poly(lactide-*co*-glycolide); Hydroxyapatite; Surface grafting reaction; Composite; Preparation method

Student Number: 2017-25623

CONTENTS

Chapter 1

Introduction, Literature reviews and Objectives

1. Introduction	2
1.1. Biomedical implants	2
1.2. Biodegradable polymers for biomedical implants	7
1.3. Biocomposites with bioceramics for biomedical implants	9
1.4. Grafting as a means of surface modification	11
2. Literature reviews	13
2.1. Surface modification of hydroxyapatite with graft polymers	13
2.2. Preparation and characterization of PLA/HA biocomposites	15
2.3. Preparation and characterization of PLGA/HA biocomposites	17
3. Objectives	19
3.1. Enhancing the interfacial adhesion between polymer and fillers	19
3.2. Improving thermal, mechanical and viscoelastic properties of biocomposites	20
3.3. Manufacturing biocomposites with different preparation methods	21

Chapter 2

Surface modification of hydroxyapatite with PLGA

1. Experimental	23
1.1. Materials	23
1.2. Grafting reaction of PLGA on the surface of HA	26
1.3. Characterization of the PLGA-g-HA particles	27
1.3.1. TGA	27
1.3.2. GPC measurements	28
1.3.3. FTIR spectroscopy	29
1.3.4. Solid-state NMR spectroscopy	30

1.3.5. SEM observation	31
1.3.6. XRD spectroscopy	32
2. Results and Discussion	33
2.1. Thermogravimetry	33
2.2. Molecular weight distributions	43
2.3. FTIR spectra	52
2.4. Solid-state NMR spectra	57
2.5. Microscopic images	62
2.6. XRD patterns	65
3. Conclusion	69

Chapter 3

Thermal, mechanical and viscoelastic properties of PLGA/HA composites with different preparation methods

1. Experimental	71
1.1. Preparation of the PLGA/PLGA-g-HA composites	71
1.2. Characterization of the PLGA/PLGA-g-HA composites	72
1.2.1. DSC	72
1.2.2. Tensile testing	73
1.2.3. DMA	74
2. Results and Discussion	75
2.1. Thermal properties	75
2.2. Mechanical properties	79
2.3. Viscoelastic properties	83
3. Conclusion	89

References

List of Tables

Table 1. Basic properties of PLGA used in this study

Table 2. Basic properties of HA used in this study

Table 3. Thermogravimetry of neat PLGA, non-grafted HA and PLGA-g-HA powders

Table 4. Molecular weights of neat PLGA and 1st supernatant of PLGA-g-HA

Table 5. IR absorptions of common functional groups

Table 6. ^1H and ^{31}P chemical shifts and FWHM of non-grafted HA and PLGA-g-HA

Table 7. Crystallite size and fraction crystallinity of non-grafted HA and PLGA-g-HA powders

Table 8. Thermal properties of neat PLGA, PLGA/HA and PLGA/PLGA-g-HA composites

Table 9. Viscoelastic properties of neat PLGA, PLGA/HA and PLGA/PLGA-g-HA composites

List of Figures

Figure 1. Structure and tears of anterior cruciate ligament (ACL):

- (a) Knee bones and ligaments
- (b) ACL tears

Figure 2. Structure and tears of rotator cuff:

- (a) Four rotator cuff muscles
- (b) Rotator cuff tears

Figure 3. Arthroscopic surgery for torn tendon using implant fixations:

- (a) Graft tendon method for torn ACL reconstruction
- (b) Suture anchor repair for torn rotator cuff reconstruction

Figure 4. Commercially used interference screws:

- (a) Metal interference screws
- (b) Bioabsorbable interference screws (Bioscrews)

Figure 5. Biodegradable polymers for biomedical application

Figure 6. Bioceramics for biomedical application

Figure 7. Classification of grafting methods

Figure 8. TGA isothermal test at 200 °C for 1 h:

- (a) TGA isothermal test of HA
- (b) TGA isothermal test of PLGA

Figure 9. TGA thermograms of PLGA-grafted HA with different ratios:

(a) PLGA:HA = 10:90

(b) PLGA:HA = 20:80

(c) PLGA:HA = 30:70

(d) PLGA:HA = 50:50

Figure 10. Tendency of grafted weight fractions:

(a) Grafted weight fractions as a function of reaction time

(b) Grafted weight fractions as a function of PLGA ratio

Figure 11. Scheme of grafting reaction in terms of grafted weight fraction

Figure 12. TGA thermograms of neat PLGA, non-grafted HA, and PLGA-g-HA powders

Figure 13. DTG thermograms of neat PLGA, non-grafted HA, and PLGA-g-HA powders

Figure 14. Molecular weights and polydispersity indices of neat PLGA as a function of reaction time

Figure 15. Molecular weight distributions of PLGA-grafted HA with different ratios:

(a) PLGA:HA = 10:90

(b) PLGA:HA = 20:80

(c) PLGA:HA = 30:70

(d) PLGA:HA = 50:50

Figure 16. Tendency of molecular weights:

(a) Molecular weights as a function of reaction time

(b) Molecular weights as a function of PLGA ratio

Figure 17. Scheme of grafting reaction in terms of molecular weight

Figure 18. Molecular weight distributions of neat PLGA and 1st supernatant of PLGA-g-HA

Figure 19. FTIR spectra of PLGA-grafted HA (30:70) with different reaction time:

- (a) FTIR spectra change with different reaction time
- (b) Enlargement of FTIR spectra near 1720 cm^{-1} (C=O bond)

Figure 20. FTIR spectra of neat PLGA, non-grafted HA, and PLGA-g-HA powders

Figure 21. Scheme of grafting reaction of PLGA on the surface of HA

Figure 22. Solid-state ^1H NMR spectra of non-grafted HA and PLGA-g-HA powders

Figure 23. Solid-state ^{31}P NMR spectra of non-grafted HA and PLGA-g-HA powders

Figure 24. SEM micrographs of non-grafted HA and PLGA-grafted HA powders

($\times 100,000$):

- (a) Non-grafted HA
- (b) PLGA-grafted HA (30:70) reacted for 3 min
- (c) PLGA-grafted HA (30:70) reacted for 5 min
- (d) PLGA-grafted HA (30:70) reacted for 10 min
- (e) PLGA-grafted HA (30:70) reacted for 30 min
- (f) PLGA-grafted HA (30:70) reacted for 60 min
- (g) PLGA-grafted HA (30:70) reacted for 120 min

Figure 25. Powder XRD patterns of non-grafted HA and PLGA-grafted HA

powders:

(a) Powder XRD patterns with different reaction time

(b) Peak comparison between HA and PLGA-g-HA

Figure 26. DSC thermograms of neat PLGA, PLGA/HA, and PLGA/PLGA-g-HA

composites:

(a) First heating scan

(b) Second heating scan

Figure 27. Representative stress-strain curves of neat PLGA, PLGA/HA, and

PLGA/PLGA-g-HA composites

Figure 28. Tensile strengths, elongations at break, and elastic moduli of neat PLGA,

PLGA/HA, and PLGA/PLGA-g-HA composites

Figure 29. DMA thermograms of neat PLGA, PLGA/HA, and PLGA/PLGA-g-HA

composites:

(a) Storage modulus

(b) Loss modulus

(c) Tan delta

Chapter 1

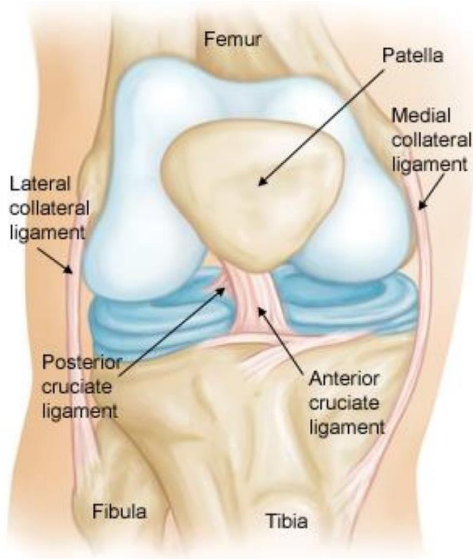
Introduction,
Literature Reviews and
Objectives

1. Introduction

1.1. Biomedical implants

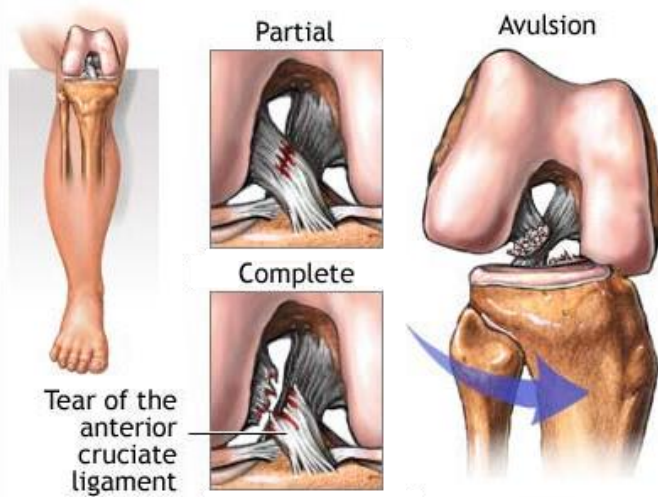
Tendon tears such as rotator cuff tears and cruciate ligament tears often occur due to excessive or repetitive loads on shoulders and knees, which cause pain and dysfunction, as shown in Figure 1 and 2. These tears require surgical reconstruction involving fixation of tendon to proximal bone in order to hold the torn tendon tight in place until it is biologically healed (Cummins, Strickland et al. 2003), as shown in Figure 3. The ideal fixture for torn tendon should have enough mechanical strength to allow for rehabilitation exercises, sustain the musculoskeletal system until the complete healing occur, and be easily handled for surgery (Lee, Mahar et al. 2005). In the past, transosseous tunnels and suture anchors were used to repair a torn tendon. With the transition from open surgery to arthroscopic repair, medical metal implant (Figure 4(a)) was initially introduced. However, this kind of implant had several complications; Metal anchor is not bioabsorbable so that it would be left untouched even after healing process is completely done and could also cause a local inflammatory reaction around the implant. This indicates that the use of metal anchors involves subsequent revision surgery to remove retained anchors. Moreover, metal anchor interferes with postoperative magnetic resonance imaging (MRI) evaluation which monitors the adjacent tissue and bone reactions during the healing process (Barber, Elrod et al. 1995, Pawaskar, Kekatpure et al. 2015). Biodegradable polymer-based anchor as known as 'bioscrew' (Figure 4(b)) was introduced to overcome the shortcomings of the metal anchor. It has enough mechanical strength to fix torn tendon and sufficient sustained strength until complete healing. Due to its biodegradability, there is no requirement to involve subsequent revision surgery because it is gradually bioabsorbed after fulfilling its biomechanical function. Due to its biocompatibility, it is more suitable for recently attempted suture-less arthroscopic surgery which is to fix directly the rotator cuff to the proximal humerus without the arthroscopic difficulties of guiding sutures through tendon and tying secure knots. Furthermore, polymer anchor cause little interference for postoperative advanced imaging techniques in contrast with metal anchor (Lee, Mahar et al. 2005). Because of these practical advantages, bioabsorbable polymer-based anchors have been prevalingly utilized for biomedical implants.

(a)



(<https://goo.gl/images/d1DZXT>)

(b)

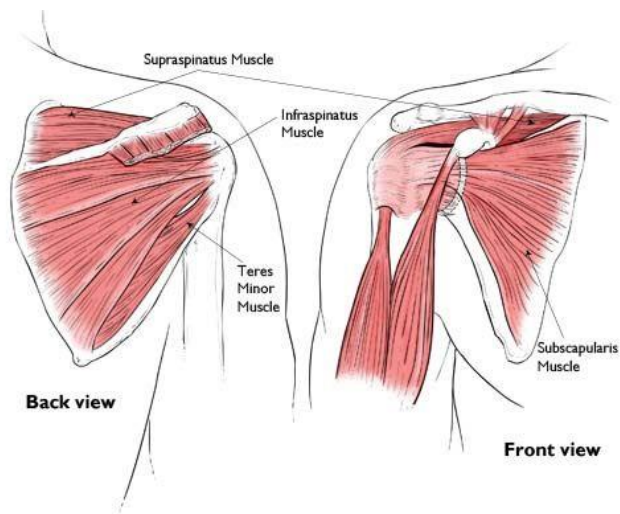


(<https://www.orthoindy.com>)

Figure 1. Structure and tears of anterior cruciate ligament (ACL):

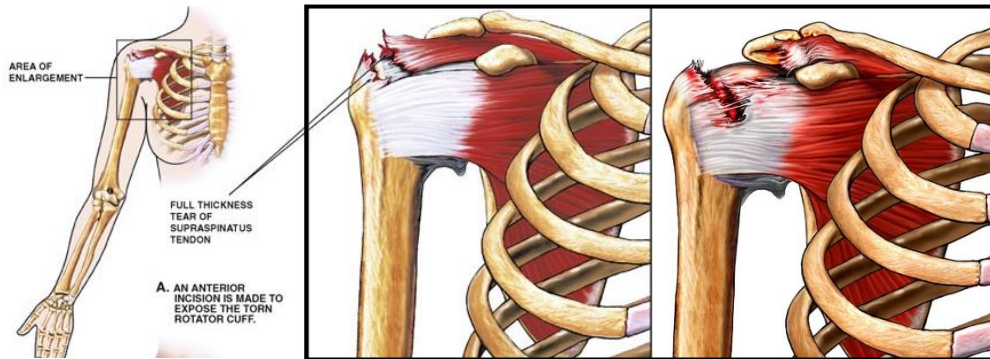
- (a) Knee bones and ligaments
- (b) ACL tears

(a)



(<https://goo.gl/images/6a19bQ>)

(b)



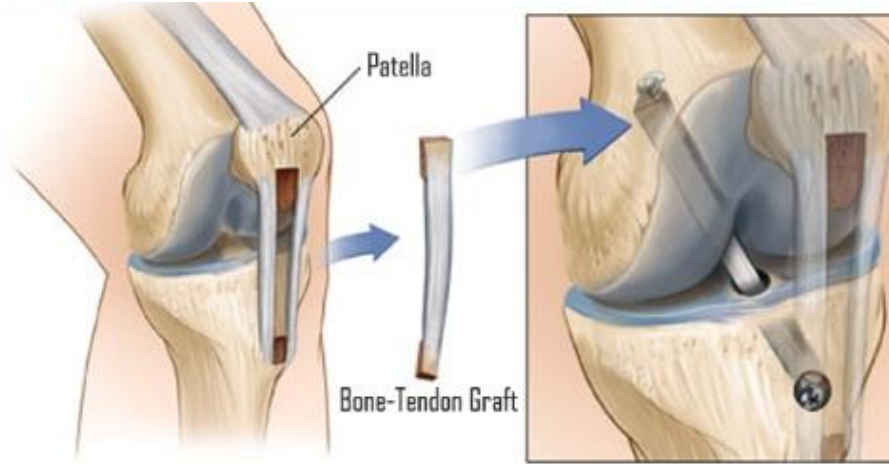
(<https://goo.gl/images/CSfCRE>)

Figure 2. Structure and tears of rotator cuff:

(a) Four rotator cuff muscles

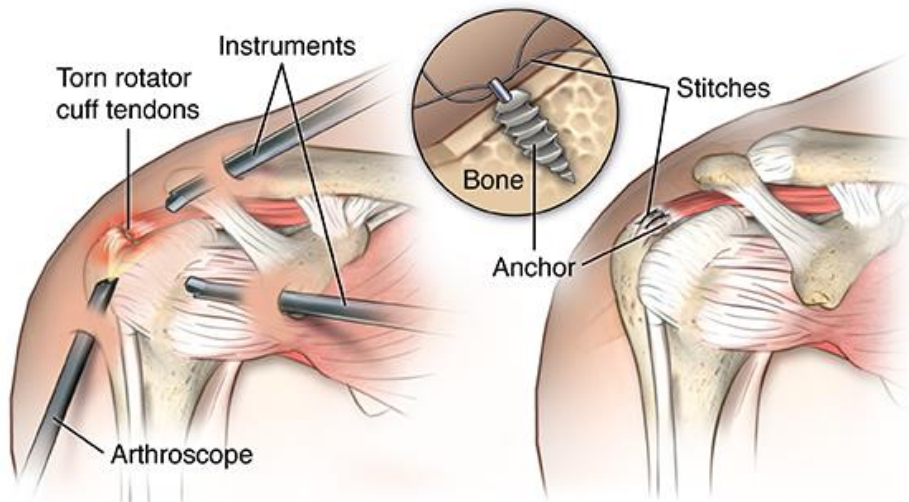
(b) Rotator cuff tears

(a)



(<https://goo.gl/images/1jaz1V>)

(b)



(<https://goo.gl/images/eyxvPE>)

Figure 3. Arthroscopic surgery for torn tendon using implant fixations:

(a) Graft tendon method for torn ACL reconstruction

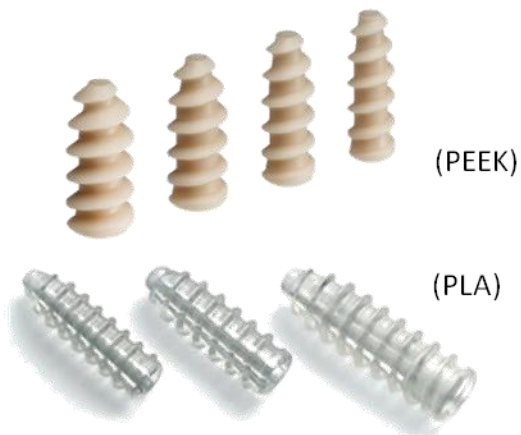
(b) Suture anchor repair for torn rotator cuff reconstruction

(a)



(<https://goo.gl/images/GQwtik>)

(b)



(<https://goo.gl/images/jjbLaK>)
(<https://goo.gl/images/2VYuZr>)

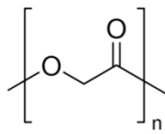
Figure 4. Commercially used interference screws:

(a) Metal interference screws

(b) Bioabsorbable interference screws (Bioscrews)

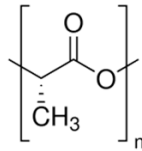
1.2. Biodegradable polymers for biomedical implants

Much research on medical implants has attempted to create effective bone substitutes. Metal implants comprising stainless steel, Ti, and Co–Cr alloys are often used because they show good mechanical properties, but their high elastic moduli can damage adjacent bone. To resolve this problem, replacements based on polymers and ceramics have been developed. Representative polymers for biomedical application are presented in Figure 5. Biodegradable polymers such as poly(glycolic acid) (PGA), poly(L-lactic acid) (PLLA), and poly(D,L-lactic acid) (PDLLA) have been extensively used in the last two decades (Hong, Zhang et al. 2005, Erbetta, Alves et al. 2012). However, while PLLA experiences slow biodegradation because of its hydrophobicity, hydrophilic PGA biodegrades quickly. PDLLA has much poorer mechanical properties than PGA or PLLA because it is amorphous in nature. Therefore, poly(lactide-*co*-glycolide) (PLGA) was introduced to overcome these inherent disadvantages of PGA and PLLA. PLGA can be used for many biomedical applications because its mechanical strength and degradation rate can be modulated by manipulating the molecular weights and ratios of lactide and glycolide units (Nair and Laurencin 2007, Phua, Roberts et al. 2011, Azimi, Nourpanah et al. 2014). PLGA has been used as both porous scaffold structures (Ren, Ren et al. 2005, Hu, Gu et al. 2014) and electrospun fibers (Song, Ling et al. 2013). However, this biodegradable polymer retains problems such as low biocompatibility and rapid losses in strength with degradation.



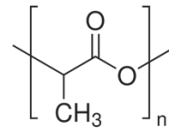
Poly(glycolic acid)
(PGA)

- Quick biodegradation due to hydrophilicity



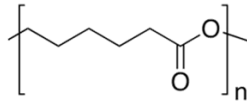
Poly(L-lactic acid)
(PLLA)

- Good mechanical properties due to crystallinity
- Slow biodegradation due to hydrophobicity



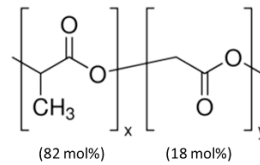
Poly(D,L-lactic acid)
(PDLLA)

- Poor mechanical properties due to amorphous nature



Poly(ε-caprolactone)
(PCL)

- Low mechanical properties



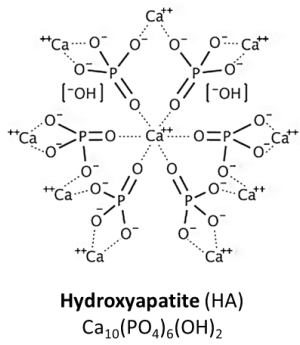
Poly(lactide-co-glycolide)
(PLGA)

- **Good mechanical properties**
- **Controllable biodegradation rate**

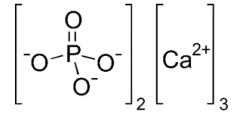
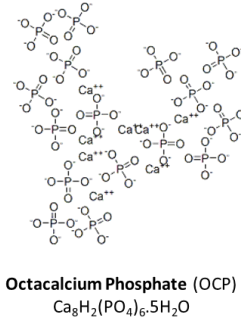
Figure 5. Biodegradable polymers for biomedical application

1.3. Biocomposites with bioceramics for biomedical implants

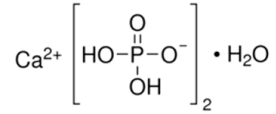
Bioceramics such as hydroxyapatite (HA) and β -tricalcium phosphate (β -TCP) have also attracted attention for medical purposes. Representative bioceramics for biomedical application are presented in Figure 6. HA is especially widely used as a bone substitute because it shows outstanding biocompatibility, originating from its chemical and crystallographic similarities to natural bone. HA also has advantages like non-toxicity, osteoconductivity, and osteoinductivity (Murugan and Rao 2003, Hong, Qiu et al. 2004, Hong, Zhang et al. 2005, Degirmenbasi, Kalyon et al. 2006). However, pure HA bioceramic is limited in applicability because it is fragile and non-biodegradable. To obtain all the advantages of biodegradable polymers and bioceramics simultaneously, composites of these two material types were developed. PLA/HA composites have attracted significant attention because they show good osteoconductivity, osteoinductivity, biodegradability, and mechanical strength; many medical products using these composites have been commercialized. However, they continue to show poor mechanical properties because insufficient interfacial adhesion between HA particles and the polymer matrix causes interfacial failure in the composite (Hong, Qiu et al. 2004, Qiu, Hong et al. 2005). To enhance interfacial adhesion, the surface of HA has been modified with various materials such as silane coupling agents (Borum and Wilson 2003), zirconyl salts (Misra 1985), polyacids (Liu, Bakker et al. 1998), polyethylene glycol (Wang, Li et al. 2002), isocyanate (Liu, de Wijn et al. 1998), and Sr (Wong, Wong et al. 2009). The grafting-based polymerization of L-lactide with stannous octanoate catalyst was introduced to modify HA surfaces with PLLA (Hong, Qiu et al. 2004, Qiu, Hong et al. 2005).



- **Good cell attachment and proliferation**
- Biocompatibility but no Bioresorbability
- Fragile
- Hard to plasticize



Tricalcium Phosphate (TCP)
 $\text{Ca}_3(\text{PO}_4)_2$



Dicalcium Phosphate Dihydrate (DCPD)
 $\text{CaHPO}_4 \cdot \text{H}_2\text{O}$

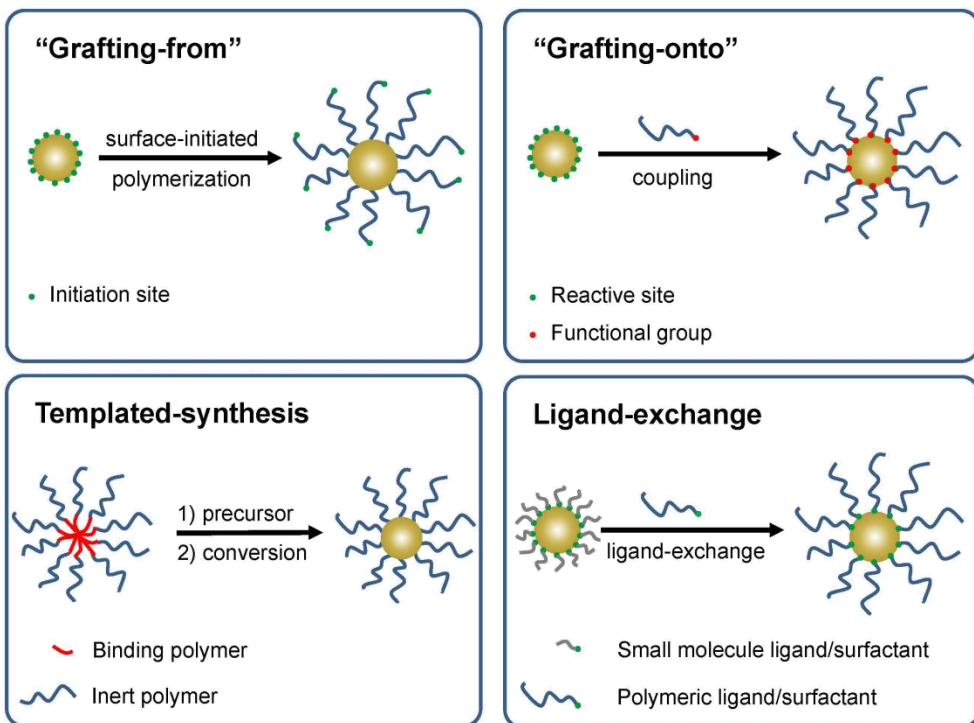
Calcium Phosphate Ceramics

- **Biocompatibility and Bioresorbability**
- Too fast bioresorbable before healing

Figure 6. Bioceramics for biomedical application

1.4. Grafting as a means of surface modification

Surface modification is one of the efficient techniques that can assign novel functionality or reactivity to materials. For polymer composites, surface modification of fillers improves the interfacial adhesion with polymer matrix, which leads to enhanced properties. Surface grafting method is one of the chemical surface modification methods and classified into several categories in Figure 7. Compared with physical modification methods such as coating and deposition, the covalent linkages of polymer chains are formed on the surface of materials. Grafting methods can be divided into three classes; grafting-to, grafting-from, and grafting-through. Grafting-to method is the coupling reaction between surface functional groups of the materials and preformed polymer chains carrying reactive end-functional groups. This method requires existing reactive groups or generation of new reactive sites by other surface treatments. For graft copolymers, free-radical polymerization, anionic polymerization, and atom-transfer radical polymerization (ATRP) are commonly used. Grafting-from method is the graft polymerization from the reactive initiating functionality of the materials. The initiating sites can be incorporated by copolymerization, additional chemical reactions, or can already exist on the surface of the materials. This method can be classified as chemical, radiation, photochemical, and plasma-induced according to the different methods used for the generation of reactive groups (Xu, Huang et al. 2009). Free-radical polymerization, anionic polymerization, and atom-transfer radical polymerization (ATRP) are also commonly used for grafting-from method. Grafting-through, also known as macromonomer method, is the copolymerization using well-defined acrylate-functionalized macromonomers and initiators. It is known as the one of the simplest ways to synthesize well-defined graft copolymers. In this method, the reactivity ratio of the end-functional groups on the macromonomers to the monomers controls the formation of heterogeneous or homogeneous branches (Ito, Tsuchida et al. 1985). Appropriate grafting method can lead to surface modification of fillers for polymer composites.



(<https://www.cmu.edu>)

Figure 7. Classification of grafting methods

2. Literature reviews

2.1. Surface modification of hydroxyapatite with graft polymers

Aissa, Debbabi et al. (2007) investigated the reaction between phenyl phosphonic dichloride and synthetic calcium hydroxy- and fluorapatite. The evidence of grafted mono- or polymeric phenyl phosphonic groups to hydroxyapatite was confirmed using FTIR and solid-state ^{31}P NMR spectroscopy, which contained phosphate groups of hydroxyapatite and grafted phenyl phosphonic groups, respectively. After grafting reaction, powder XRD analysis showed preserved apatitic structures of HA. This analysis could be utilized for me to prove the grafted materials consisting of HA. In contrast, fluorapatite showed no reaction with phenyl phosphonic groups. They proposed the reaction mechanism between phenyl phosphonic dichloride reagent and hydrogen phosphate ion and hydroxide of HA.

Liu, de Wijn et al. (1998) introduced the surface modification method of nanoscale hydroxyapatite using hexamethylene diisocyanate as a coupling agent. They proved that hydroxyl groups at the surface of nano-apatite have reactivity towards organic functional groups. Polyethylene glycol chains grafted onto the surface of HA were characterized using FTIR and solid-state ^1H MAS NMR spectroscopy; FTIR spectra showed the formation of urethane and ether linkages on the surface of HA and solid-state ^1H NMR spectra showed the reduction of the amount of hydroxyl groups. The weight percentage of grafted polymer was determined using total organic carbon analysis (TOC) and TGA. Their results indicate the chemical reactivity towards isocyanate groups and how to calculate the amount of grafted polymers in weight.

Hong, Qiu et al. (2004) attempted the grafting ring-opening polymerization of L-lactide onto the surface of hydroxyapatite nanoparticles. PLLA was directly grafted onto HA surface through a chemical linkage and PLLA-g-HA particles were stably dispersed in organic solvents. PLLA-g-HA particles showed downfield displacement in ^{31}P MAS NMR spectra compared with that of pure HA. Phosphate groups of HA did not participate in the reaction but it seemed that surface grafting affected the chemical environment. This indicates ^{31}P MAS NMR could be one of useful methods to figure out the grafting reaction. FTIR spectra

confirmed the existence of surface-grafted PLLA. The amount of grafted polymer was determined using TGA. PLLA/PLLA-g-HA composites displayed increasing tensile strength and elongation at break.

Qiu, Hong et al. (2005) developed the novel surface modification of hydroxyapatite nanoparticles by surface grafting reaction of L-lactic acid and ring-opening polymerization of L-lactide with a stannous octanoate catalyst. They obtained HA modified by L-lactic acid and PLLA-grafted HA. The modified surface of HA was analyzed using FTIR, ³¹P MAS NMR spectroscopy and TGA. The results showed that HA reacts easily with L-lactic acid and successful graft polymerization of L-lactic acid was initiated by hydroxyl groups of grafted L-lactic acid. The grafting amount was calculated using TGA. They also prepared modified HA/PLLA composites, which displayed enhanced mechanical properties and uniform microstructures.

Wang, Dai et al. (2010) prepared the scaffolds consisting of hydroxyapatite or poly(ϵ -caprolactone)-grafted HA and poly(ϵ -caprolactone) (PCL) by using the thermally induced phase separation/salt leaching technique. PCL-grafted HA particles were evaluated using FTIR and TGA as the same way mentioned above. Grafting reaction on the surface of HA was also confirmed using powder XRD patterns. Through the introduction of grafted HA particles, mechanical strength, porosity and thermal property were modified. Especially, the compressive modulus of composite scaffold was highly enhanced.

2.2. Preparation and characterization of PLA/HA biocomposites

Hong, Zhang et al. (2005) examined to prepare the PLLA-grafted HA/PLLA composites to improve the bonding between HA and PLLA, which leads to a increase of mechanical properties. Thermal properties were investigated using DSC and the structure of the composites was studied using SEM, polarized optical microscopy (POM) and cell culture. PLLA chains grafted on the HA surface improved the interfacial adhesion between polymer matrix and particles. PLLA-grafted HA had a role of toughening effect of composites, which exhibited remarkably increasing mechanical properties such as the elastic modulus.

Jose, Thomas et al. (2009) synthesized aligned nanofibrous scaffolds consisting of PLGA and HA nanoparticles by electrospinning for bone tissue engineering. Through the morphological characterization, average fiber diameter was controlled according to the amounts of HA nanoparticles. There were no agglomerates at low HA content, which means good dispersion. However, excessive HA content resulted in broken fibers due to agglomeration. This indicates the importance of dispersion when it comes to composites. From DSC results, it is found that well-dispersed HA particles are involved in the chain mobility. The viscoelastic properties and degradation characteristics of the scaffolds were also investigated. A suitable amount of HA made the composites less degradable and had higher modulus.

Xiao, Li et al. (2007) introduced the surface modification of PLA with poly(α -methacrylic acid) (PMAA) via photo-oxidation and UV-induced polymerization in order to control the growth of HA crystals and improve the interfacial interaction between two phases. It was confirmed that PMAA polymer chains were grafted onto the PLA surface and grafting rate increased with reaction time by using FTIR spectroscopy. The composites were synthesized by blending PMAA-modified PLA and HA nanoparticles. Though powder XRD and SEM observation, PMAA-modified PLA could manipulate the morphology as well as the nucleation and growth of HA crystals and affect the dispersion of fillers.

Li, Lu et al. (2008) attempted the surface modification of HA particles by ring-opening polymerization of lactide. The surface modification was characterized chemically and quantitatively using FTIR and TGA, respectively. These analyses confirmed the graft

polymerization of lactide onto the surface of HA. Measuring mechanical properties of PLA-grafted HA/PLA composites, they found that the introduction of surface modification of HA enhanced the adhesion between HA particle and PLA matrix and modified HA particles were more well-dispersed in PLA matrix.

2.3. Preparation and characterization of PLGA/HA biocomposites

Petricca, Marra et al. (2006) synthesized PLGA/HA composites by a colloidal non-aqueous chemical precipitation technique in the presence of the solubilized polymer. The microstructure of the scaffold indicates a homogenous distribution of HA particles in the PLGA polymer matrix. Bonding characteristics between HA and PLGA, the microstructure, tensile strength, and thermal stability of the composites were investigated. It showed suitable mechanical properties as bone substitution scaffolds. In vitro studies were conducted for osteoblast-like adhesion assessment on composites utilizing MG63 cells. The incorporation of the sufficient amount of HA could maximize the osteoconductivity of the composites.

Cui, Liu et al. (2009) investigated the surface modification of nanohydroxyapatite with L-lactic acid oligomers. HA/PLGA nanocomposites with different HA contents were fabricated into the scaffolds by the melt-molding and particulate leaching methods. L-lactic acid oligomers were grafted onto the surface of nanohydroxyapatite. HA particles could disperse uniformly and have the interconnected pore structures. HA/PLGA composites exhibited good biocompatibility, homogeneity and mechanical properties. Through the animal test, it was confirmed that cell attachment and proliferation, and osteogenetic ability of composites were influenced by HA content. They optimized the composite as the bone repairing materials for tissue engineering and orthopedic application even with histological analysis.

Zhang, Hong et al. (2009) fabricated a three-dimensional porous scaffold with the composite of PLGA and PLLA-grafted HA nanoparticles, using the solvent casting and particulate leaching method. This paper is interesting in that graft polymer is PLLA but polymer matrix consists of PLGA. After surface modification, PLLA-grafted HA particles were more uniformly dispersed and showed a lower calcium exposure on the composite surface. The intramuscular implant study showed that PLLA-grafted HA/PLGA scaffold was more stable than that of HA/PLGA and similar postoperative biodegradability and mineralization to HA/PLGA up to the HA content. For repairing critical radius defects, PLLA-grafted HA/PLGA scaffold exhibited rapid and strong osteoconductivity. The incorporation of bone morphogenetic protein 2 (BMP-2) to the composite implant could enhance the osteogenic process. It is concluded that PLLA-grafted HA/PLGA implant could play a role to guide the new bone formation with the intact adjacent structure.

Song, Ling et al. (2013) prepared the composites of PLLA-grafted HA particles and PLGA by electrospinning as the materials for new biodegradable guided bone regeneration (GBR) membranes. The composite fiber membranes were investigated at length including mechanical properties, wettability, degradation, bioactivity, and biocompatibility. PLLA-grafted HA/PLGA composites showed enhanced mechanical strength with appropriate PLLA-grafted HA content while excessive filler content led to the deterioration of properties due to the agglomeration of fillers. Wettability, degradation, and bioactivity also depended upon PLLA-grafted HA content. To assess the biocompatibility of the composite fiber membranes, the cell attachment test was conducted and it resulted that the osteoblasts adhered well and spread rapidly than the control. These results suggested that the bioresorbable PLLA-g-HA/PLGA composite fiber membranes could be utilized for GBR therapy.

3. Objectives

3.1. Enhancing the interfacial adhesion between polymer and fillers

Hydroxyapatite is one of the inorganic materials but PLGA consists of organic carbon-based polymer chains. The biocomposite of PLGA and HA was introduced to utilize both biodegradability of PLGA and biocompatibility of HA. For impeccable biocomposite, PLGA and HA should be well blended and tightly combined. However, just blending two different materials without chemical linkage formation shows little compatibility. PLGA polymer matrix and HA particles are separated and there are fatal cracks between their interfaces. Therefore, surface modification of HA will be introduced by PLGA-grafting reaction to increase their compatibility. PLGA polymer chains would be chemically grafted on the surface of HA, which have the role to entangle with polymer matrix and compatibilize HA particles in the matrix through van der Waals force and hydrogen bonding. This indicates the improvement of the interfacial adhesion between polymer matrix and inorganic fillers for polymer composites. The grafting reaction will be confirmed using FTIR and solid-state NMR spectroscopy. The grafted weight fraction will be analyzed using TGA and molecular weight change of polymer chains will be indirectly checked using GPC. SEM observation and XRD analysis will be conducted to examine morphological characteristics after grafting.

3.2. Improving thermal, mechanical and viscoelastic properties of biocomposites

Surface modification of HA particles by grafting PLGA polymer chains increases entanglement with PLGA polymer matrix. The enhanced interfacial adhesion between PLGA and PLGA-grafted HA strengthens the entire biocomposites, which leads to improvement of thermal, mechanical and viscoelastic properties; The introduction of thermally stable inorganic fillers and tight entanglement via surface modification impedes the thermal degradation and makes the biocomposites more thermoresistant. Chemically bonded PLGA polymer chains entangle throughout the biocomposites and hold them tight, which causes the enhanced mechanical properties such as tensile strength, flexural strength and impact strength with any external loads. Similarly, lengthy polymer chains and well-woven entanglement induce the viscoelastic performance such as modulus and damping. Therefore, thermal, mechanical and viscoelastic properties will be investigated respectively for prepared biocomposites; Transition temperatures such as glass transition temperature will be measured using DSC. Tensile strength, elongation and elastic modulus will be measured using UTM. Storage modulus, loss modulus and damping factor will be measured using DMA.

3.3. Manufacturing biocomposites with different preparation methods

For polymer composites, the interfacial adhesion is one of the most important factors to affect their properties. Because surface modification of HA is introduced to enhance the interfacial adhesion between PLGA polymer matrix and HA particles, it is necessary to evaluate performance improvement of surface grafting reaction. In this study, specimens will be prepared by injection molding with and without surface modification; PLGA/HA composite and PLGA/PLGA-g-HA composite. Meanwhile, the dispersion of fillers is one of the most important factors to affect their properties as well as the interfacial adhesion. PLGA/PLGA-g-HA composites will be classified according to three different blending methods before injection molding; the extrusion molding using a twin-screw compounding extruder, simple blending of milled PLGA and PLGA-g-HA powders, and the re-dispersion of PLGA-g-HA powders into PLGA matrix using a solvent. Specimens will also be prepared using injection molding after each blending method. Comparing thermal, mechanical and viscoelastic properties of biocomposites by above-mentioned measurements, the influence of dispersion for biocomposites will be examined.

Chapter 2

Surface modification of hydroxyapatite with PLGA

1. Experimental

1.1. Materials

PLGA (L-lactide:glycolide = 82:18) was produced by Corbion Purac (Netherlands). It has an inherent viscosity of 1.8 dL g^{-1} in chloroform, a maximum degradation time of 6 months, and a melting range of 127.5 to 141.4 °C. The number-average molecular weight (M_n) of PLGA is $\sim 130,000$. HA was purchased from Sigma-Aldrich and used as filler. Basic properties of PLGA and HA are presented in Table 1 and 2, respectively. Chloroform (99.8% purity) was purchased from Samchun Pure Chemical (Republic of Korea) and used as a solvent.

Form	Amorphous
Feed ratio	Lactide : Glycolide = 82 : 18
Molecular weight	M _w 220,000-250,000
Degradation timeframe	< 6 months
Viscosity	0.55-0.75 dL/g, 0.1 % (w/v) in chloroform (25 °C)
Transition temp	T _g 45-50 °C
Solubility	ethyl acetate, chloroform, acetone and THF: soluble
Storage temp	2-8°C

Table 1. Basic properties of PLGA used in this study

Abbreviation	HAp, HA
Category	Phosphate mineral apatite group
Repeating Unit	$\text{Ca}_5(\text{PO}_4)_3(\text{OH})$
Molecular Weight	1004.6 g/mol
Crystal System	Hexagonal

Table 2. Basic properties of HA used in this study

1.2. Grafting reaction of PLGA on the surface of HA

In a 100-mL vial, PLGA was dissolved in chloroform by magnetic stirrer with stirring rate of 800 rpm at 50 °C for 6 h. After the PLGA pellets were dissolved, HA was added and the mixture was blended by magnetic stirrer with stirring rate of 600 rpm at 50 °C for 6 h. The ratios of PLGA:HA mixture were 10:90, 20:80, 30:70, and 50:50. To obtain a uniform dispersion of HA with the polymer chains, the PLGA/HA suspension was sonicated using POWERSONIC 410 (40 kHz, Hwashin Instrument Co., Ltd., Republic of Korea) at room temperature (25 °C, RT) for 3 h and poured into an Al dish. After drying at 50 °C for 6 h to remove the chloroform, the Al dish was placed in a high-temperature oven at 200 °C to react HA and PLGA. The reaction time was 3, 5, 10, 30, 60, and 120 min. The reacted mixture was transferred to a conical tube, dispersed in chloroform by sonication at RT for 3 h, and then separated into the first supernatant and sediment by centrifuging at 3,000 rpm for 10 min. The first supernatant was moved to a separate vial and the first sediment was re-dispersed in chloroform by sonication at RT for 3 h before separation into the second supernatant and sediment by centrifugation at 3,000 rpm for 10 min to completely remove non-grafted PLGA polymer chains. The vial containing the first supernatant and the conical tube containing the second sediment were dried at 50 °C for 24 h to remove residual chloroform. After drying, the supernatant was weighed to create a solution of equal concentration for GPC molecular weight measurement. After centrifuging and drying, the sediment was referred to as PLGA-grafted HA.

1.3. Characterization of the PLGA-g-HA particles

1.3.1. TGA

Thermogravimetric analysis was performed using a TGA 4000 (PerkinElmer, USA) to determine the occurrence of grafting and measure the weight of PLGA grafted onto the HA surface qualitatively. Samples weighing 15 to 20 mg were loaded in the chamber with 20.0-mL/min N₂ used as the purge gas. After holding for 1 min at 30 °C, temperature scanning from 30 to 700 °C proceeded at the heating rate of 10 °C/min. The TGA furnace was then cooled by a water-circulating device. The grafted weight fraction was calculated using the following equation:

$$\text{GWF (\%)} = W_{\text{R,HA}} (\%) - W_{\text{R,g-HA}} (\%)$$

where $W_{\text{R, HA}}$ is the residue weight percentage of HA and $W_{\text{R, g-HA}}$ is the residue weight percentage of PLGA-grafted HA. The residue weight percentages were determined by TGA.

1.3.2. GPC measurements

The oven-dried supernatant was dissolved in tetrahydrofuran (THF) and sonicated at RT for 30 min to create a 1.5-wt% solution. The molecular weights were measured using a YL9100 GPC System (YoungLin Instruments, Republic of Korea) equipped with a YL9170 refractive index (RI) detector. GPC columns were eluted with 35 °C THF as an eluent solvent at a flow rate of 1 mL/min. The number-average (M_n) and weight-average (M_w) molecular weights were calculated using a calibration curve from polystyrene standards.

1.3.3. FTIR spectroscopy

Infrared (IR) spectra were obtained using an FT/IR-6100 (JASCO, Japan) equipped with a Mylar beam splitter and an attenuated total reflectance (ATR) accessory composed of a diamond crystal with a 45° angle of incidence. Spectra were collected from 4000 to 400 cm^{-1} 32 times at the resolution of 4 cm^{-1} . The grafting reaction of PLGA was characterized by monitoring the changes in the C=O bond peak at ~1735–1750 cm^{-1} . All spectra were corrected through CO₂ reduction, H₂O reduction, noise elimination, and baseline correction.

1.3.4. Solid-state NMR spectroscopy

Solid-state ^1H NMR spectra were obtained through a 500-MHz solid NMR system using a BRUKER AVANCE II 500 spectrometer (BRUKER, Germany) with cross-polarization (CP) and the magic-angle spinning (MAS) technique. The spectrometer was operated at the Larmor frequency of 500.13 MHz in a 4-mm CP/MAS probe head. The spinning frequency of MAS was 10 kHz and the 90° pulse length was 3.3 μs ; 32 scans were recorded with a recycle delay of 3 s. For solid-state ^{31}P NMR spectra, the spectrometer was operated at the Larmor frequency of 202.45 MHz in a 4-mm CP/MAS probe head. The spinning frequency of MAS was 10 kHz and the 90° pulse length was 2.0 μs ; 256 scans were recorded with a recycle delay of 1 s.

1.3.5. SEM observation

SEM imaging was conducted using a SUPRA 55VP FESEM (Carl Zeiss, Germany) to characterize the morphology of PLGA-grafted HA particles. After oven-drying at 50 °C for 24 h, the particles were fixed with C tape on a Cu-based stub and coated with a thin layer of Pt at a sputter current of 30 mA for 140 s. The microscopy was performed at an accelerating voltage of 2 kV and working distance of 3.6 mm.

1.3.6. XRD spectroscopy

XRD patterns were obtained using an Ultima III Powder X-Ray Diffractometer (Rigaku, Japan) to determine the crystalline structures of the PLGA-grafted HA powders. The powders were well compressed on the sample holder. The diffractometer used Cu K α radiation ($\lambda = 1.54 \text{ \AA}$) at 40 kV and 30 mA from a fixed graphite monochromator. The Bragg angle (2θ) range was scanned from 2° to 60° at a rate of $2^\circ/\text{min}$ with a step size of 0.02° . The crystallite sizes (D) of HA and PLGA-g-HA powders were determined using the diffraction peak of (002) planes and Scherrer's equation:

$$D = K\lambda/\beta\cos\theta$$

where D is the average crystallite size, β is the full width of the peak at half of the maximum intensity (FWHM, in radians), λ is the irradiation wavelength (1.540562 \AA), and K is a constant related to the crystallite shape, here approximated as unity.

The crystalline fractions (X_c) of the HA and PLGA-grafted HA powders were determined using the following equation:

$$X_c = (K_A/\beta)^3$$

where β is the FWHM (in degrees) of the peak and K_A is a constant set at 0.24.

2. Results and Discussion

2.1. Thermogravimetry

TGA isothermal tests were conducted to confirm the thermal stability of PLGA and HA as shown in Figure 8. The tests were carried out at 200 °C for 1 h. HA had no weight loss and PLGA also had few (0.3%) weight loss, which indicates PLGA and HA are thermally stable enough not to affect calculating the grafted weight fractions (GWFs) of PLGA-grafted HA powders.

TGA thermograms of PLGA-grafted HA with different ratios are presented in Figure 9: (a) PLGA:HA = 10:90, (b) PLGA:HA = 20:80, (c) PLGA:HA = 30:70, and (d) PLGA:HA = 50:50. The final weights at ~700 °C decreased with increasing reaction time, which means HA reacted more with PLGA polymer chains. The final weights also decreased with increasing HA ratios. The higher HA ratio is, the more decomposition of PLGA grafted onto the HA surface occurs during the TGA test. The tendency of grafted weight fractions is summarized in Figure 10. As shown in Figure 10(a), the GWFs generally increased with increasing reaction time, which indicates the grafting reaction occurred more and more PLGA polymer chains grafted to the surface of HA. Meanwhile, when the ratios of PLGA:HA are 20:80, 30:70 and 50:50, the GWFs are converging to the one point. The GWFs show different tendency with different PLGA ratios in Figure 10(b), which means PLGA:HA ratio is one of the important factor to decide the grafted weight fractions. In case of the ratio of PLGA:HA is 50:50, the initial GWF is lower than that of the ratio of 30:70 and the GWF gradually increases. This slow initial grafting is attributed to relatively low amounts of HA compared to other cases. The scheme of grafting reaction was presented in terms of grafted weight fraction in Figure 11. When the reaction time increases, it is expected that grafting ratio increases and grafted chain length decreases. The combination with grafting ratio and grafted chain length determines the GWF value. The condition with the ratio of 30:70 and the reaction time of 30 min shows the maximum GWF value, which is the optimal condition to be referred to as “PLGA-g-HA”.

TGA and DTG thermograms of neat PLGA, non-grafted HA, and PLGA-g-HA powders are presented in Figure 12 and Figure 13, respectively, with the results summarized in Table 3. $T_{5\%}$,

$T_{10\%}$, and $T_{50\%}$ are the temperatures at which the weight losses are 5, 10, and 50 wt%, respectively. T_d is the thermal decomposition temperature and T_{max} is the temperature at the maximum rate of weight loss. W_R is the residual weight ratio after TGA measurement. As shown in Figure 12, non-grafted HA displays a total weight loss of ~4%, occurring in two steps within temperature ranges of 30 to 140 °C and 430 to 480 °C. The first stage is attributed to the evaporation of surface-adsorbed water; the second stage to the loss of bound water in the crystalline lattice (Ashok, Sundaram et al. 2003). Meanwhile, PLGA shows the onset of thermal decomposition at ~300 °C and ~100% weight loss at 700 °C as an organic polymer. Similarly, PLGA-g-HA shows onset of thermal decomposition at ~300 °C, indicating that the PLGA polymer chains grafted on the HA surface begin to decompose. According to previous studies on the surface modification of HA with PLA, high GWF values typically require long surface modification times. For example, the maximum GWF is ~6 wt% when L-lactide and HA are reacted for 18 h with a catalyst (Hong, Qiu et al. 2004) and ~21.6 wt% when PLA and HA are reacted with a catalyst (Qiu, Hong et al. 2005). Even though PLGA and HA are reacted for only 30 min with no catalyst here, however, the calculated GWF reaches 10.032 wt%. Therefore, surface grafting is confirmed quantitatively by the GWF value. As shown in Figure 13 and Table 3, PLGA-g-HA has lower T_d and T_{max} values than neat PLGA. The decrease of T_d arises from the decrease of the molecular weight (Palacio, Orozco et al. 2011), suggesting that surface grafting on HA causes PLGA chain length decreases. Because HA is highly thermally stable, PLGA-g-HA has higher $T_{5\%}$ and $T_{10\%}$ values compared to neat PLGA; however, the chain-shortening effect of HA affects the thermal and mechanical properties of the composites, as discussed later in Chapter 3.

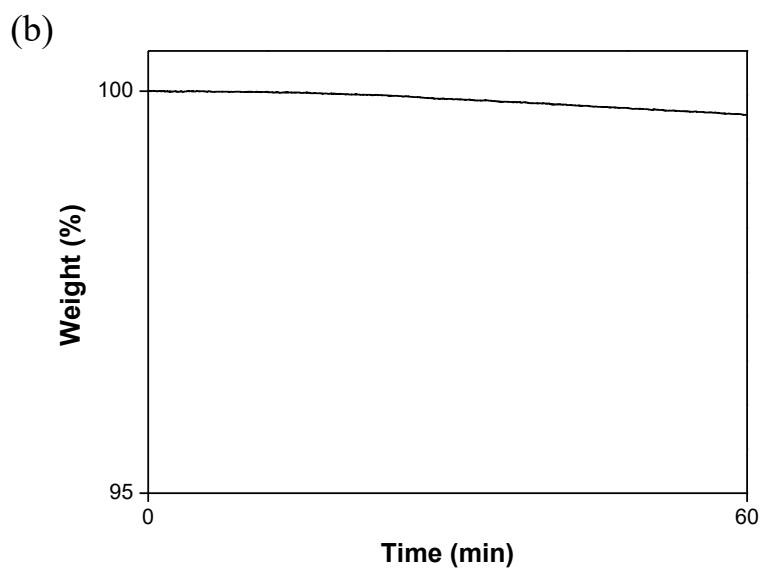
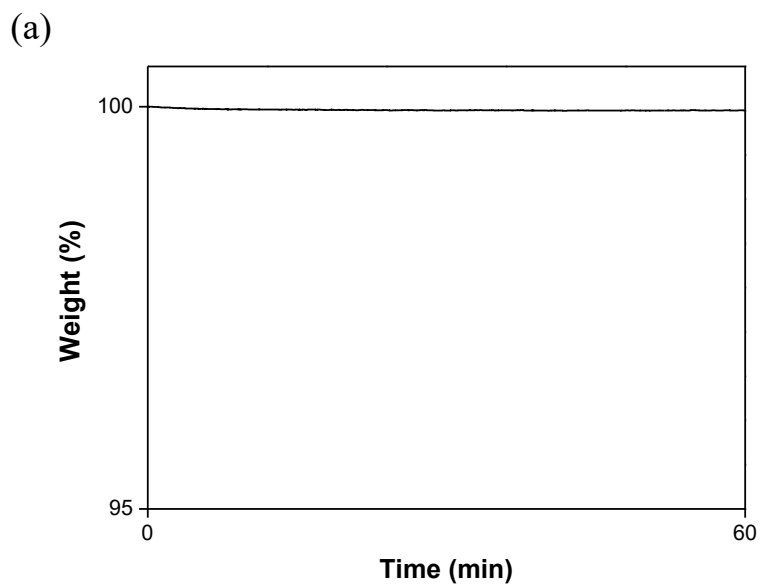
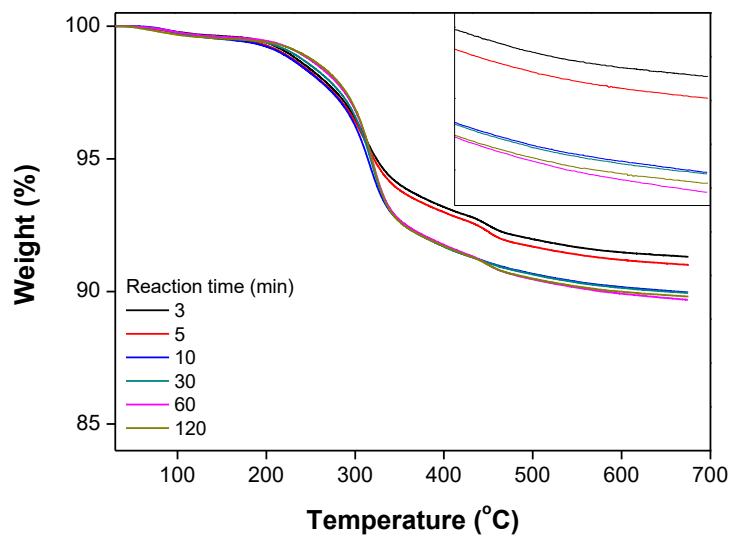


Figure 8. TGA isothermal test at 200 °C for 1 h:

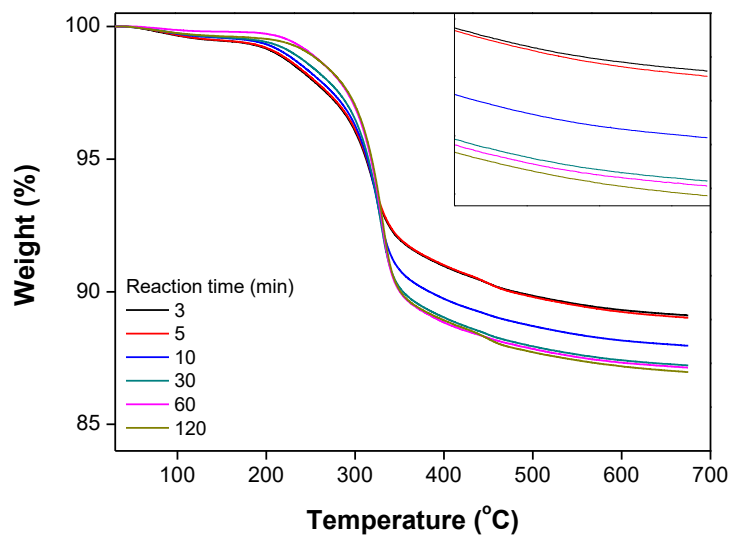
(a) TGA isothermal test of HA

(b) TGA isothermal test of PLGA

(a)



(b)



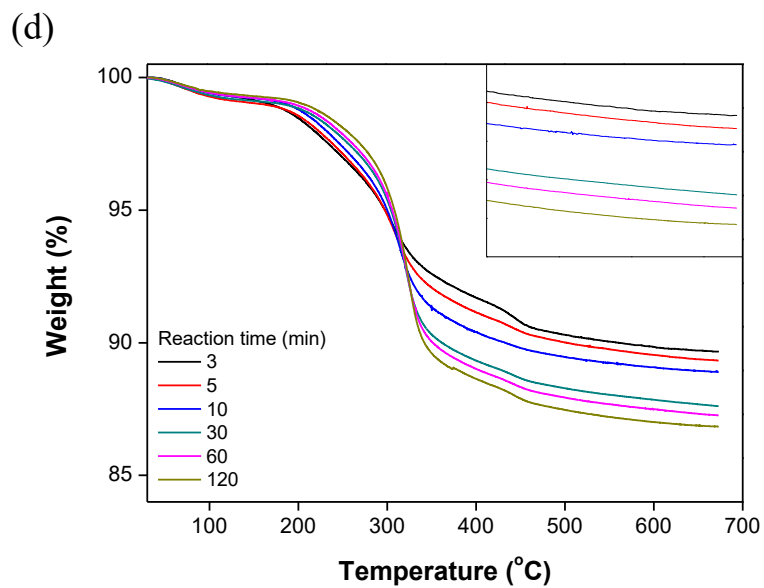
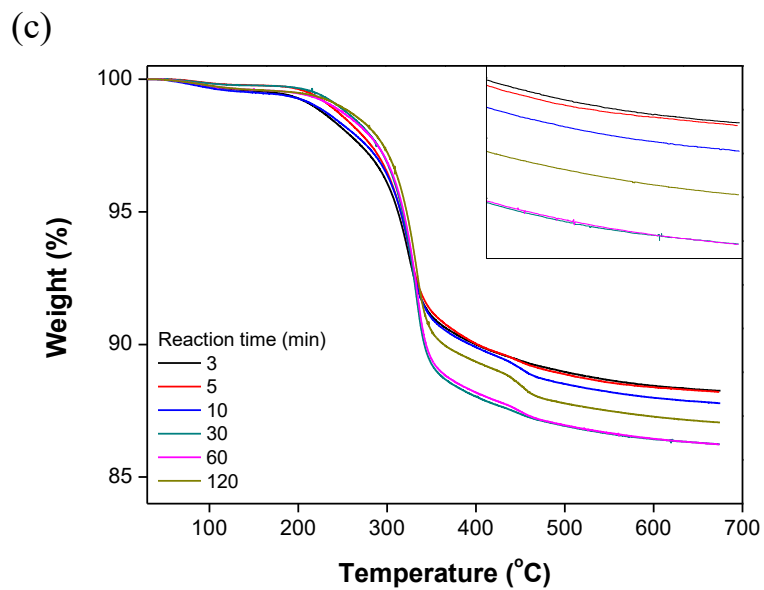
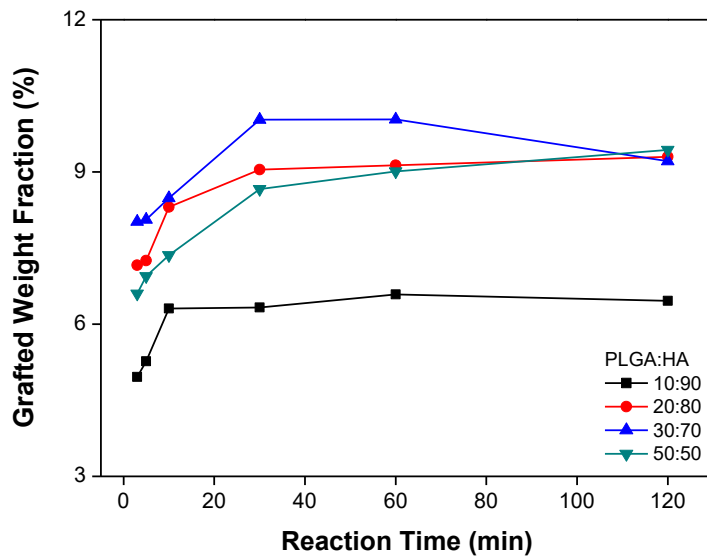


Figure 9. TGA thermograms of PLGA-grafted HA with different ratios:

- (a) PLGA:HA = 10:90
- (b) PLGA:HA = 20:80
- (c) PLGA:HA = 30:70
- (d) PLGA:HA = 50:50

(a)



(b)

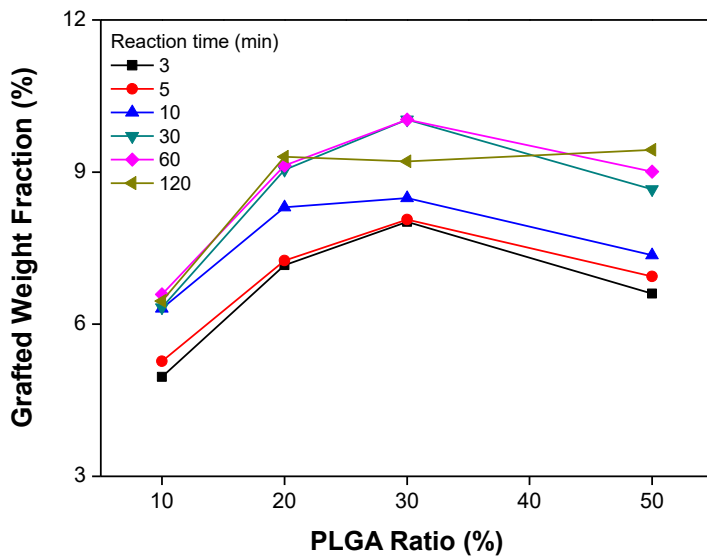


Figure 10. Tendency of grafted weight fractions:

(a) Grafted weight fractions as a function of reaction time

(b) Grafted weight fractions as a function of PLGA ratio

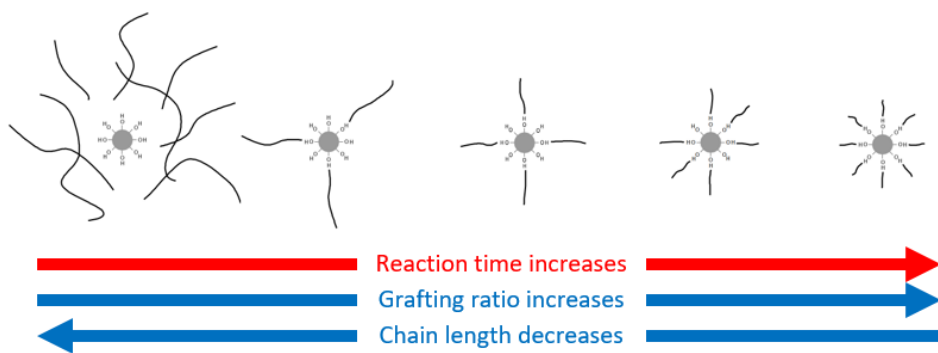


Figure 11. Scheme of grafting reaction in terms of grafted weight fraction

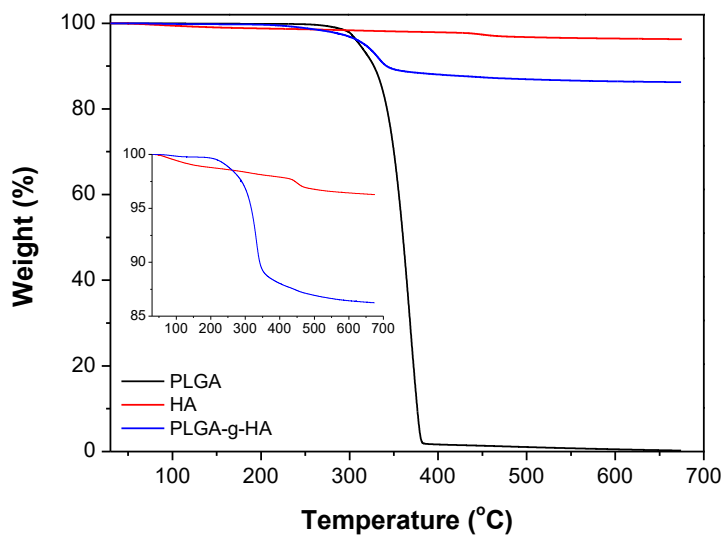


Figure 12. TGA thermograms of neat PLGA, non-grafted HA, and PLGA-g-HA powders

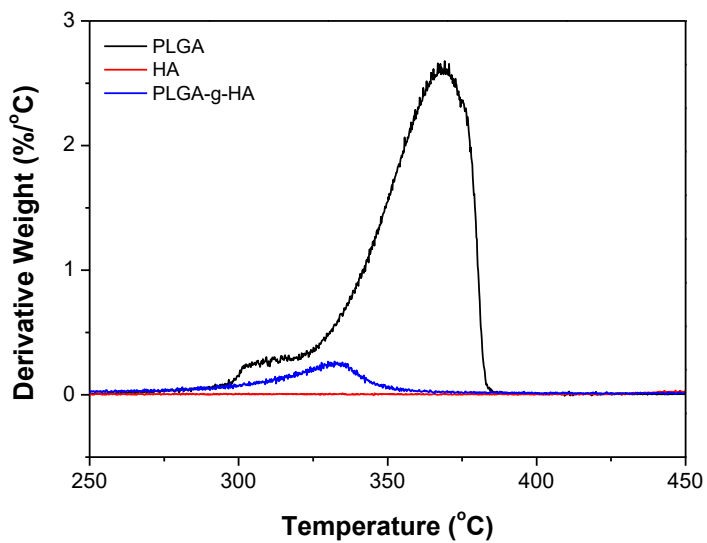


Figure 13. DTG thermograms of neat PLGA, non-grafted HA, and PLGA-g-HA powders

Table 3. Thermogravimetry of neat PLGA, non-grafted HA and PLGA-g-HA powders

	$T_{5\%}$ (°C)	$T_{10\%}$ (°C)	$T_{50\%}$ (°C)	T_d (°C)	T_{max} (°C)	W_R (wt%)
PLGA	311.60	327.57	360.31	338.77	368.52	0.229
non-grafted HA	-	-	-	-	-	96.272
PLGA-g-HA	317.32	341.94	-	297.14	333.15	86.240

2.2. Molecular weight distributions

The molecular weight was measured by GPC to determine the sizes of the PLGA polymer chains that were successfully grafted. To determine the molecular weight and polydispersity index (PDI) of the PLGA grafted on the HA surface, the first supernatant was indirectly measured (Hong, Qiu et al. 2004, Qiu, Hong et al. 2005). The molecular weights and PDI values of neat PLGA as a function of reaction time are presented in Figure 14. When the neat PLGA was thermally treated at 200 °C even without HA, Thermal decomposition of PLGA polymer chains causes decrease of the molecular weights of neat PLGA. This means thermal treatment could reduce the polymer chain length of PLGA. The PDI values increase above 2.5 because of the random occurrence of various lengths of decomposed polymer chains. It is possible to confirm the effect of reaction with HA by comparing the molecular weights with and without HA.

The molecular weight distributions of PLGA-grafted with different ratios are presented in Figure 15: (a) PLGA:HA = 10:90, (b) PLGA:HA = 20:80, (c) PLGA:HA = 30:70, and (d) PLGA:HA = 50:50. The medium values of log M (red line) shifted to the right with increasing HA ratios. Higher HA ratio causes more grafting reaction of PLGA in the TGA result, at the same time, longer grafted PLGA polymer chains. The tendency of molecular weights is summarized in Figure 16. As shown in Figure 16(a), the molecular weights generally decreased with increasing reaction time, which indicates the grafting reaction gradually involved the fragmentation of polymer chains. The molecular weights are linearly proportional to PLGA ratios in Figure 16(b). In case of the ratio of 10:90, quick reaction and fragmentation caused rapid decreases of the molecular weights. In case of the ratio of 50:50, relatively slow reaction and fragmentation occurred. This difference of reactivity is subject to the frequency in accordance with adjacent HA ratio. The scheme of grafting reaction was presented in terms of molecular weight in Figure 17. When the reaction time increases, the grafting reaction accompanies the fragmentation of PLGA and the reduction of total polymer chain length. This length decrease of adjacent chains leads to probabilistic length decrease of grafted chains.

Meanwhile, the optimal condition was referred to as “PLGA-g-HA” from TGA results. The molecular weight distributions of neat PLGA and the first supernatant of PLGA-g-HA are presented in Figure 18, with molecular weights summarized in Table 4. The molecular weight

distribution of the first supernatant contains several broad peaks, while that of PLGA has only one peak. The three regions in the PLGA-g-HA distribution indicate that the transesterification between PLGA and HA split the PLGA polymer chains. Polymer chains with M_n values of $\sim 10^3$ – 10^4 are formed by reactions occurring at the middle sections of the chains; those with M_n values below 10^3 and above 10^4 are formed by reactions at the termini of the chains. Peak (1) has a very high PDI value, indicating that the PLGA polymer chains have highly varied molecular weights after the surface grafting reaction. The GPC data indirectly confirms that the reaction with HA causes decreases in the molecular weights of PLGA and that the transesterification shortened the PLGA polymer chains grafted to the HA surface.

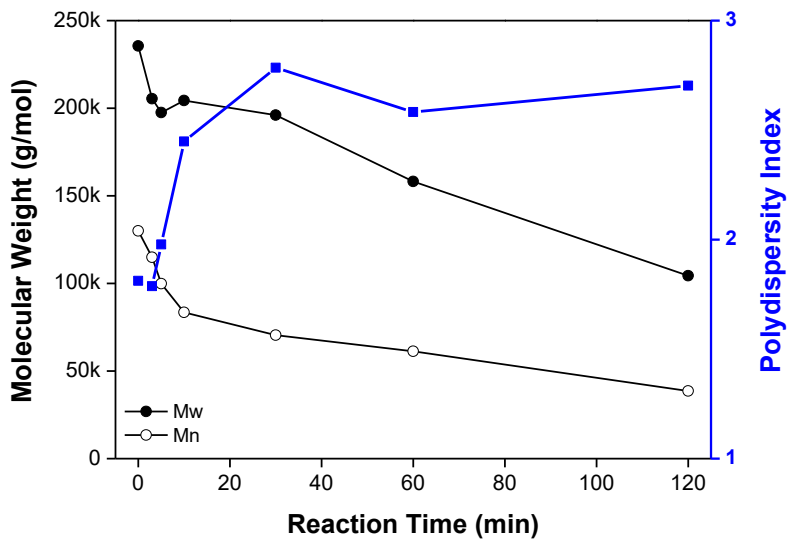
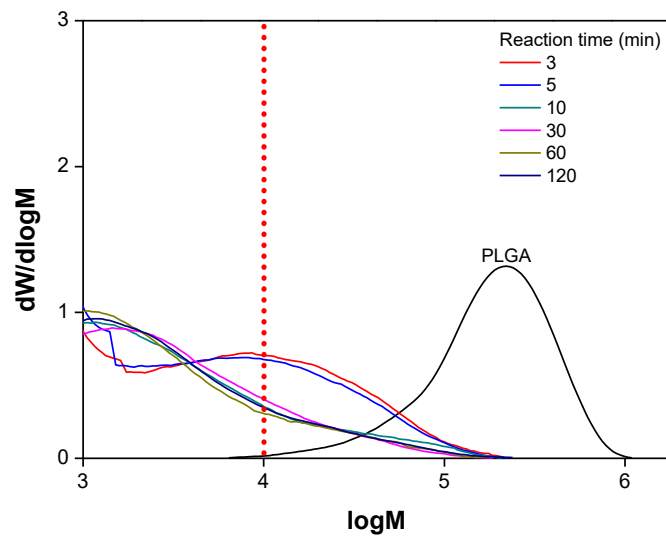
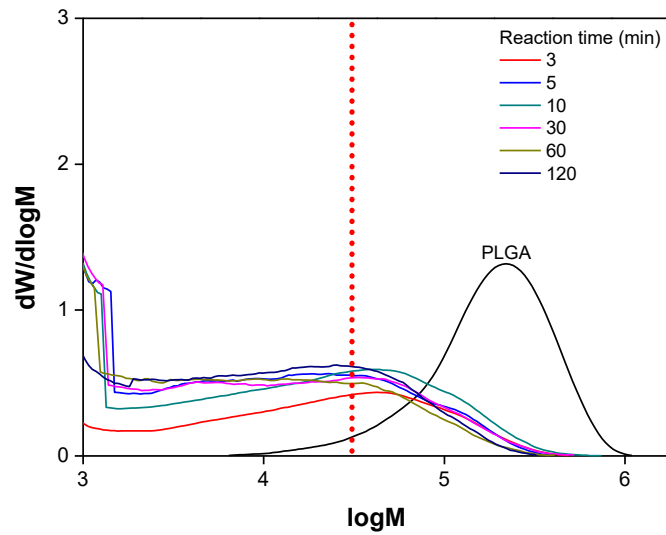


Figure 14. Molecular weights and polydispersity indices of neat PLGA as a function of reaction time

(a)



(b)



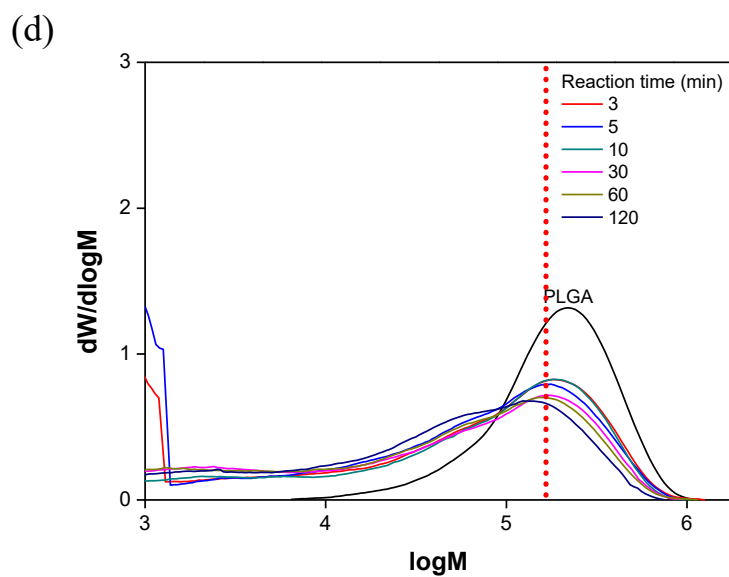
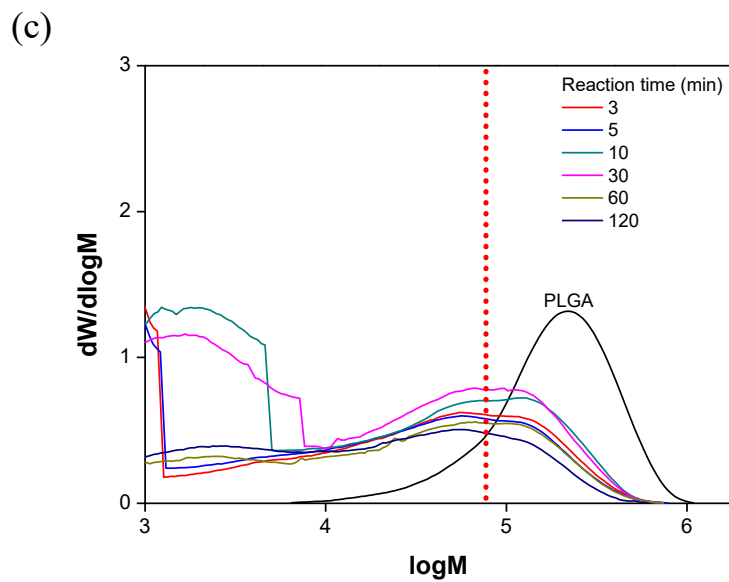
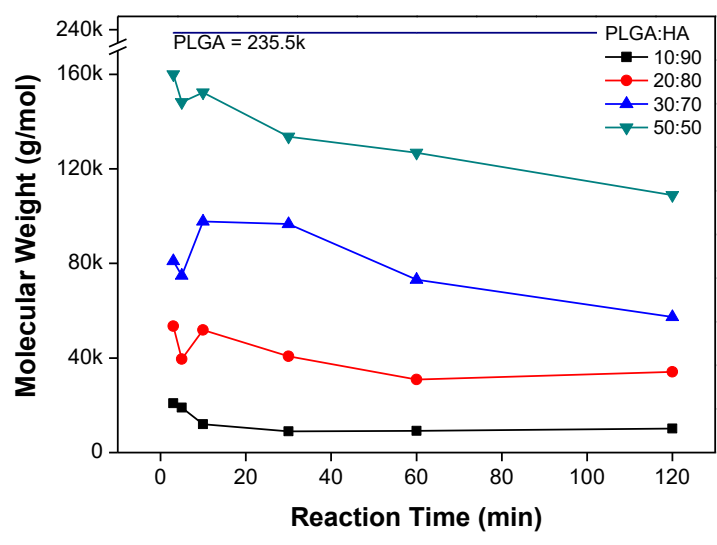


Figure 15. Molecular weight distributions of PLGA-grafted HA with different ratios:

- (a) PLGA:HA = 10:90
- (b) PLGA:HA = 20:80
- (c) PLGA:HA = 30:70
- (d) PLGA:HA = 50:50

(a)



(b)

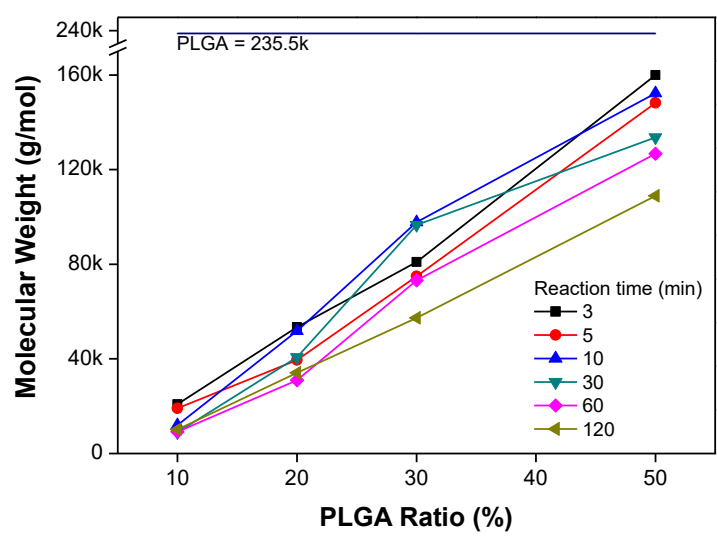


Figure 16. Tendency of molecular weights:

(a) Molecular weights as a function of reaction time

(b) Molecular weights as a function of PLGA ratio

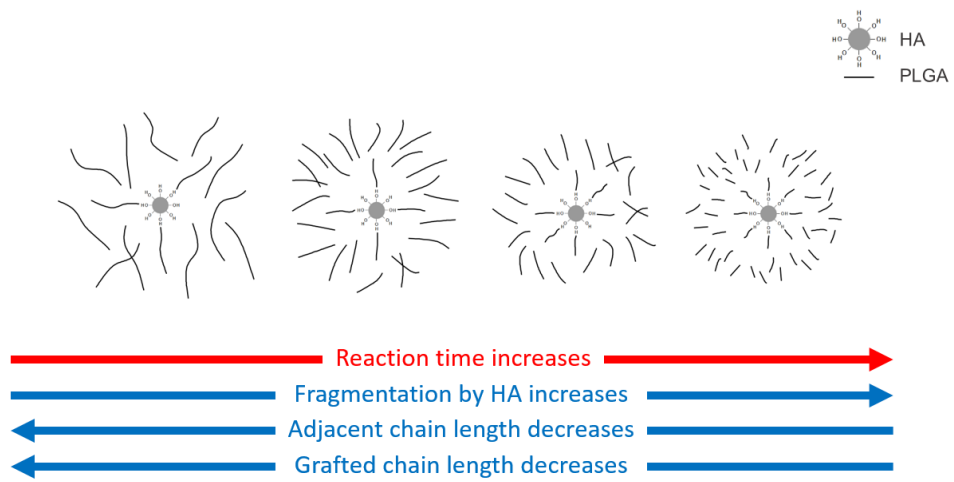


Figure 17. Scheme of grafting reaction in terms of molecular weight

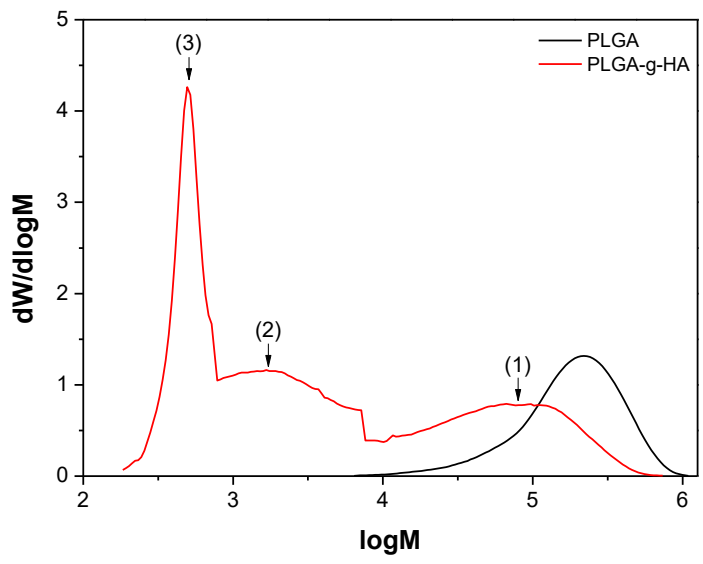


Figure 18. Molecular weight distributions of neat PLGA and 1st supernatant of PLGA-g-HA

Table 4. Molecular weights of neat PLGA and 1st supernatant of PLGA-g-HA

	Peak No.	M_n (g/mol)	M_w (g/mol)	PDI
PLGA		129,992	235,511	1.812
	(1)	37,477	96,622	2.578
PLGA-g-HA	(2)	1,859	2,753	1.481
	(3)	466	496	1.063

2.3. FTIR spectra

The FTIR spectra of PLGA-grafted HA with different reaction time are presented in Figure 19. When the reaction time increases, new peaks are gradually formed and their heights also increase (red square). From the enlargement of the spectra near 1720 cm^{-1} in Figure 19(b), the peak change occurred obviously. Through IR absorptions of common functional groups in Table 5, the bands near 1720 cm^{-1} are related to C=O bonds. It is confirmed that the grafting reaction between PLGA and HA leads to the formation of C=O linkages.

For the detailed analysis, the FTIR spectra of non-grafted HA, neat PLGA, and PLGA-g-HA are presented in Figure 20. The absorbance bands at 471, 566, 605, 963, 1031, and 1096 cm^{-1} originate from phosphate groups in the crystalline structure of HA and specifically from $\nu_2\text{ PO}_4^{3-}$ bending, $\nu_4\text{ PO}_4^{3-}$ bending, $\nu_4\text{ PO}_4^{3-}$ bending, $\nu_1\text{ PO}_4^{3-}$ stretching, $\nu_3\text{ PO}_4^{3-}$ bending, and $\nu_3\text{ PO}_4^{3-}$ bending vibrations, respectively (Chlopek, Morawska-Chochol et al. 2009, Reyes-Gasga, Martínez-Piñeiro et al. 2013). PLGA displays a large sharp absorbance band of carbonyl groups at 1750 cm^{-1} and a strong band of aliphatic C–H stretching vibrations between 3000 and 2850 cm^{-1} . In addition, distinct bands appear from asymmetric and symmetric C–O stretching vibrations between 1300 and 1150 cm^{-1} , CH_2 stretching (deformation) vibrations between 1500 and 1250 cm^{-1} , and H bonding between 3600 and 3200 cm^{-1} . Meanwhile, PLGA-g-HA shows the same peaks assigned to the bending vibrations of phosphate groups. These confirm that PLGA-g-HA contains HA, because these peaks in the PLGA-g-HA spectrum are characteristic of HA. However, two new peaks appear at 1750 and 1183 cm^{-1} for PLGA-g-HA, unlike those for non-grafted HA. As described in Figure 21, grafting of PLGA on HA occurs by esterification; that is, new ester groups are formed on the HA surface. These new absorbance bands arise from carbonyl groups and C–O bonding of PLGA in PLGA-g-HA, respectively. Furthermore, the peaks at 1747 and 1182 cm^{-1} in the PLGA spectrum are shifted to higher wavenumbers of 1750 and 1183 cm^{-1} , respectively, in the PLGA-g-HA spectrum. This shift is attributed to the decreased amount of H bonding between PLGA polymer chains from the decreased chain length and substitution that accompanies surface grafting on HA. The occurrence of the two new peaks and peak shifts confirm that the PLGA polymer chains are successfully grafted on the HA surface.

Table 5. IR absorptions of common functional groups

Functional Group		Absorption Location (cm^{-1})	Absorption Intensity
Alkane (C-H)		2850 – 2975	Medium to strong
Alcohol (O-H)		3400 – 3700	Strong, broad
Alkene	Internal (C=C)	1640 – 1680	Weak to medium
	Terminal (C=C-H)	3020 – 3100	Medium
Alkyne	Internal (C≡C)	2100 – 2250	Medium
	Terminal (C≡C-H)	3300	Strong
Nitrile (C≡N)		2200 – 2250	Medium
Aromatics		1650 – 2000	Weak
Amines (N-H)		3300 – 3350	Medium
Carbonyls (C=O)	Aldehyde (CHO)	1720 – 1740	Strong
	Ketone (RCOR)	1715	Strong
	Ester (RCOOR)	1735 – 1750	Strong
	Acid (RCOOH)	1700 - 1725	Strong

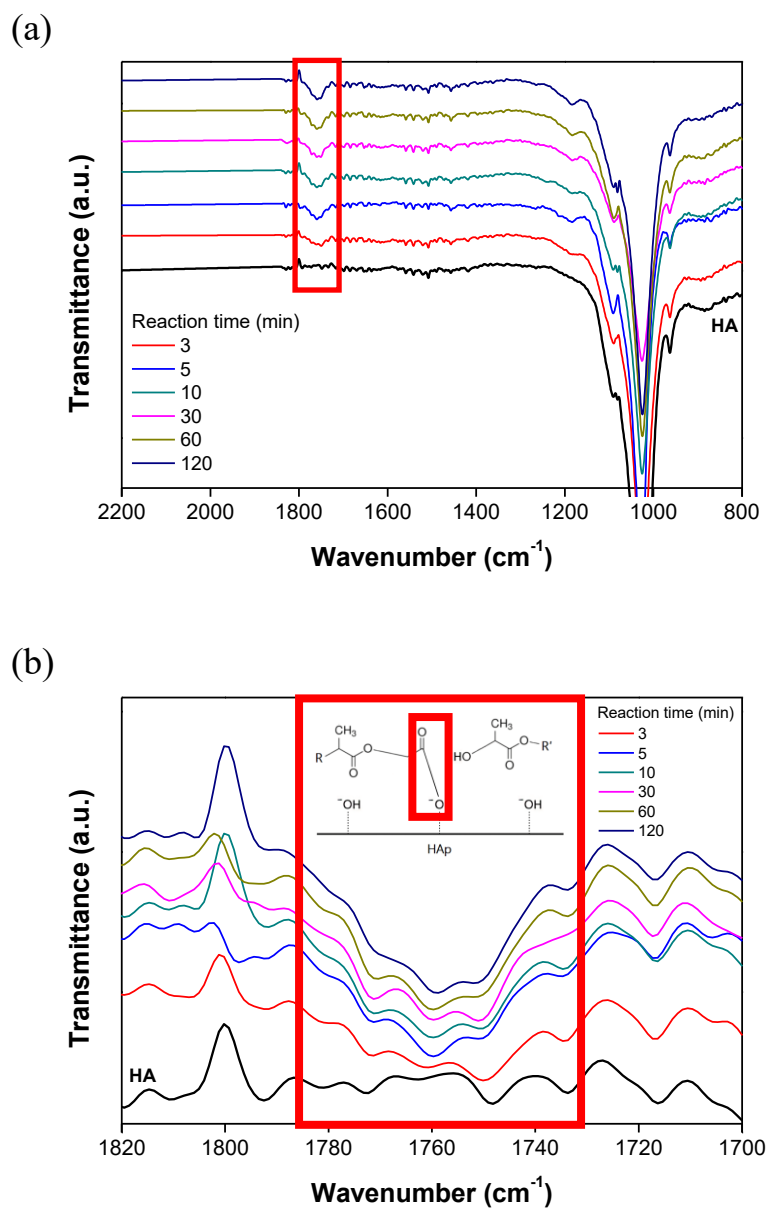


Figure 19. FTIR spectra of PLGA-grafted HA (30:70) with different reaction time:

(a) FTIR spectra change with different reaction time

(b) Enlargement of FTIR spectra near 1720 cm^{-1} (C=O bond)

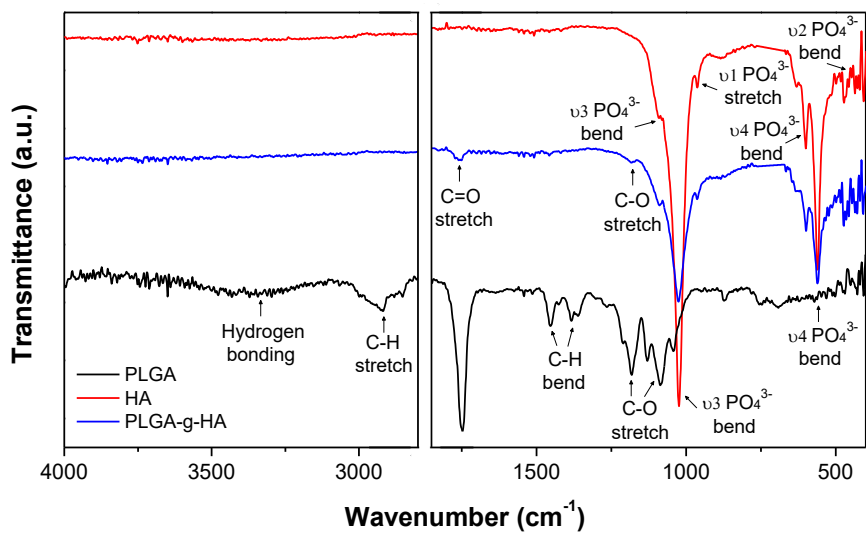


Figure 20. FTIR spectra of neat PLGA, non-grafted HA, and PLGA-g-HA powders

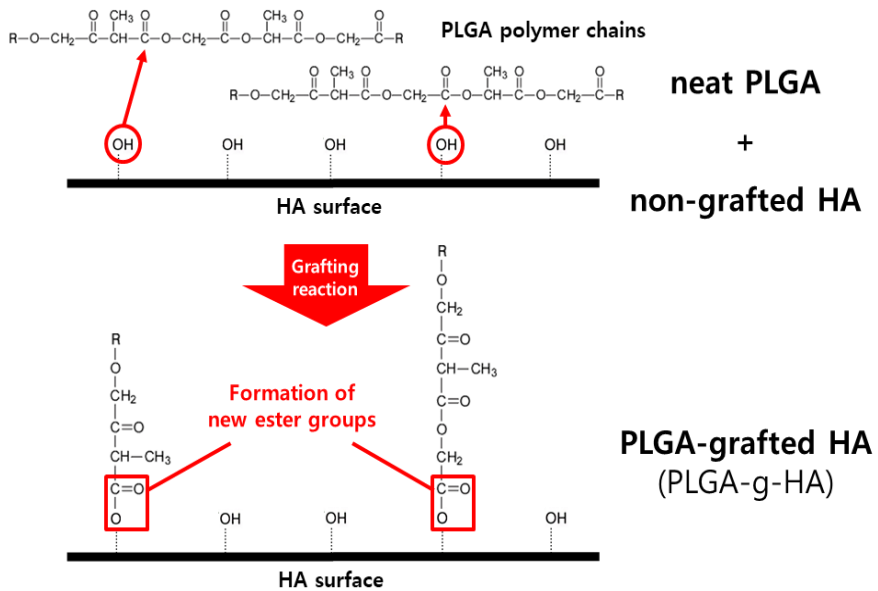


Figure 21. Scheme of grafting reaction of PLGA on the surface of HA

2.4. Solid-state NMR spectra

The ^1H NMR spectra for non-grafted HA and PLGA-g-HA are presented in Figure 22, with the main peaks of the ^1H and ^{31}P NMR measurements summarized in Table 6. The ^1H NMR spectrum of HA shows four highly intense peaks at 16.08, 13.40, 5.23, and -0.10 ppm. The peak at -0.10 ppm is assigned to protons in the structural hydroxyl groups of HA; that at 5.23 ppm is assigned to protons of water molecules adsorbed on the surface of HA (Yesinowski and Eckert 1987, Panda, Hsieh et al. 2003, Wilson, Awonusi et al. 2006). The relatively small peaks at 16.08 and 13.40 ppm are assigned to protons arising from monetite (CaHPO_4) in central planar defects (Yesinowski and Eckert 1987). After surface grafting, the two most intense peaks at 5.23 and -0.10 ppm for HA are decreased in height and shifted to 5.01 and -0.12 ppm for PLGA-g-HA, respectively. This indicates that the surface grafting reaction with PLGA reduces the amount of protons associated with free structural hydroxyl groups of HA. Furthermore, the FWHM of the peak of surface-adsorbed water is decreased significantly from 4.33 ppm for HA to 1.46 ppm for PLGA-g-HA. These changes indicate that grafting changes the chemical environment at the HA surface. The decrease in the surface-adsorbed water peak height indicates that surface hydroxyl groups act as binding sites for adjacent water molecules, and that these binding sites are blocked after grafting with PLGA polymer chains (Liu, de Wijn et al. 1998). Meanwhile, the spectrum of PLGA-g-HA has new peaks at 1.29 and 0.90 ppm compared to that of HA, suggesting that the new peaks originate from newly formed chemical bonds with PLGA. The FWHM values of these peaks are 0.92 and 1.57 ppm, respectively, which are rather large despite the low peak intensities; the peaks overlap over a broad range, suggesting that protons on the grafted PLGA exist in varied chemical environments because of interactions such as H bonding with surface-adsorbed water. The characteristic resonance peak at ~ 13 ppm can be used as a reference to compare with others because its peak intensity is unaffected by the surface grafting reaction (Liu, de Wijn et al. 1998, Choi, Lee et al. 2006, Lee, Choi et al. 2006). Therefore, the peak height of the structural hydroxyl groups at -0.10 ppm was adjusted by using the two peaks at 13.40 and 16.08 ppm as references, with peak heights calculated from the same zero value on the intensity axis. The calculated rate of peak height decrease at -0.10 ppm is 3.125% after surface grafting. This suggests that some H atoms are removed from the HA surface and surface hydroxyl groups are grafted to PLGA polymer chains.

For the ^{31}P NMR spectra as shown in Figure 23, HA and PLGA-g-HA display intense peaks at 2.68 and 2.67 ppm, respectively, arising from phosphate groups. The small peaks on the right shoulders of these intense peaks are assigned to protonated phosphate groups (Mingalyov, Kolyagin et al. 2011). While slight changes in chemical shift and FWHM appear, no distinct changes occur after the surface grafting reaction. According to previous studies on the surface modification of HA, surface grafting generally causes substantial peak changes, such as displacements in chemical shift (Hong, Qiu et al. 2004) or the formation of new peaks (Aissa, Debbabi et al. 2007) in the ^{31}P NMR spectrum. However, it seems that the surface grafting reaction of PLGA on HA has no significant influence on the chemical environment of the HA phosphate groups. Careful observation shows that the phosphate group chemical environment does change, as shown by the decreased peak heights for PLGA-g-HA.

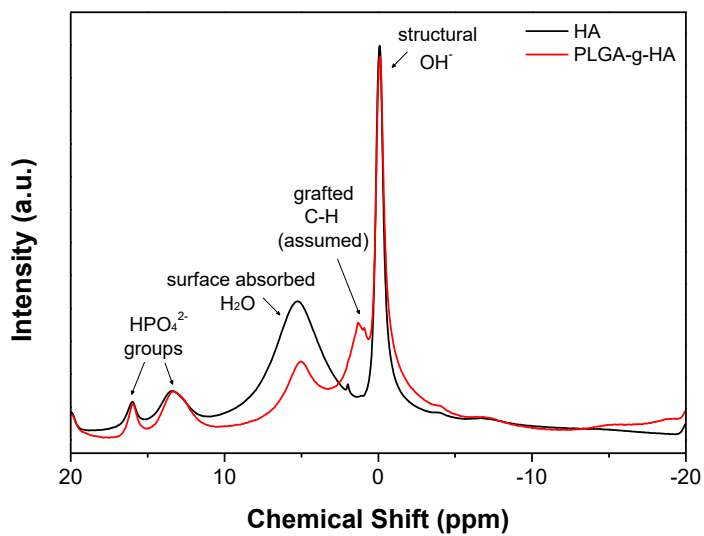


Figure 22. Solid-state ^1H NMR spectra of non-grafted HA and PLGA-g-HA powders

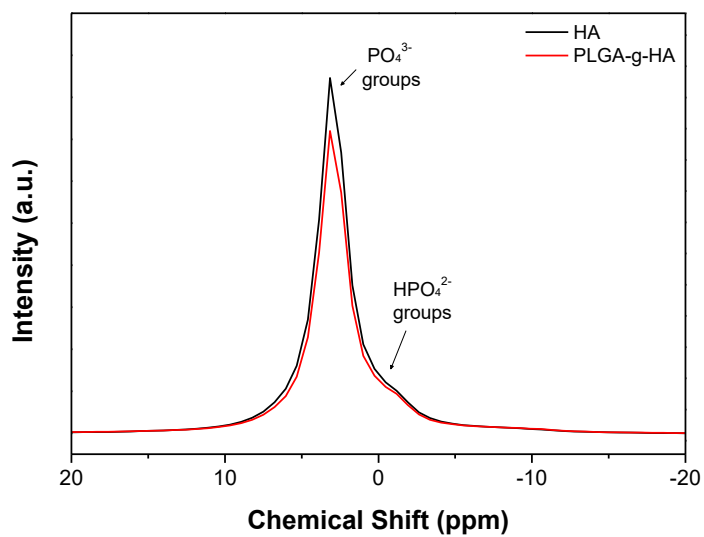


Figure 23. Solid-state ^{31}P NMR spectra of non-grafted HA and PLGA-g-HA powders

Table 6. ^1H and ^{31}P chemical shifts and FWHM of non-grafted HA and PLGA-g-HA

	^1H NMR			^{31}P NMR		
	Assignment	Chemical shift (ppm)	FWHM (ppm)	Assignment	Chemical shift (ppm)	FWHM (ppm)
non-grafted HA	OH^-	-0.10	0.68	PO_4^{3-}	2.68	1.78
	surface H_2O	5.23	4.33	HPO_3^{2-}	2.59	7.27
PLGA-g-HA	OH^-	-0.12	0.72	PO_4^{3-}	2.67	1.78
	grafted C-H	0.90	0.92	HPO_3^{2-}	2.49	7.39
	grafted C-H	1.29	1.57			
	surface H_2O	5.01	1.46			

2.5. Microscopic images

SEM micrographs of non-grafted HA and PLGA-grafted HA powders are shown in Figure 24. As shown in Figure 24(a), the HA powder shows a random distribution of nanometer-scale granular particles. Meanwhile, as shown in Figure 24(b) ~ (g), the PLGA-grafted HA powders display agglomerated structures of plate-like or rod-like clusters with some granular particles. These clusters are <100 nm in thickness. Thus, surface grafting causes morphological changes in the particles.

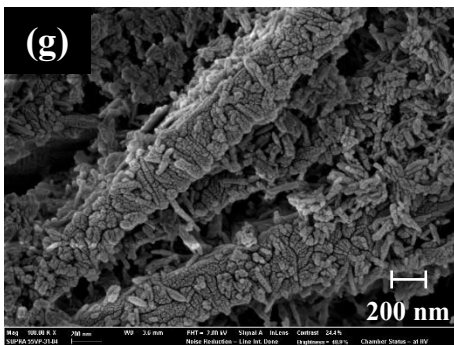
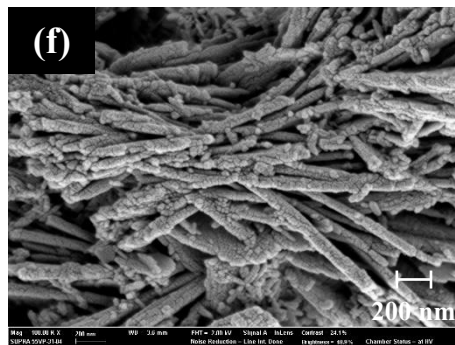
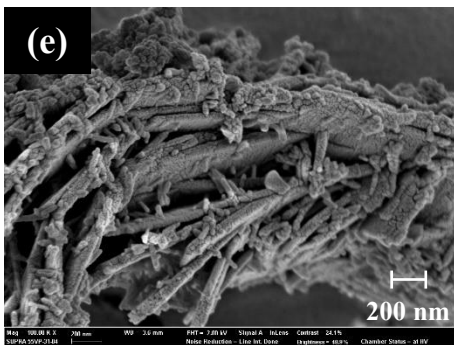
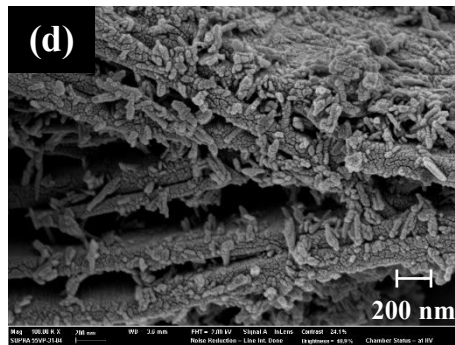
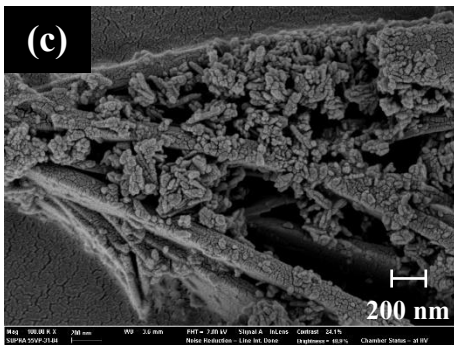
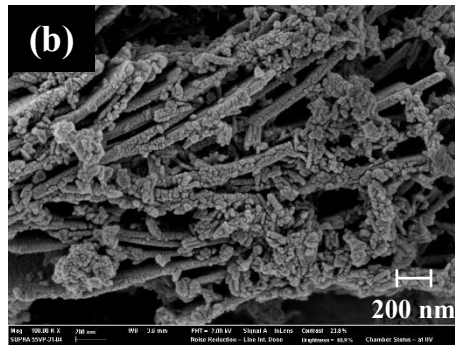
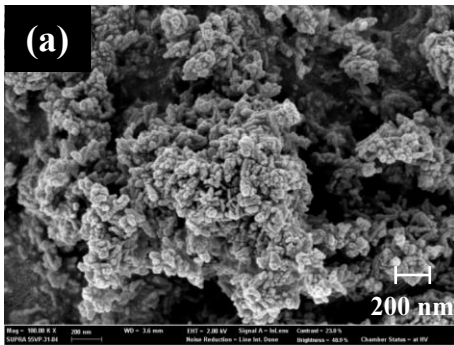


Figure 24. SEM micrographs of non-grafted HA and PLGA-grafted HA powders ($\times 100,000$):

- (a) Non-grafted HA
- (b) PLGA-grafted HA (30:70) reacted for 3 min
- (c) PLGA-grafted HA (30:70) reacted for 5 min
- (d) PLGA-grafted HA (30:70) reacted for 10 min
- (e) PLGA-grafted HA (30:70) reacted for 30 min
- (f) PLGA-grafted HA (30:70) reacted for 60 min
- (g) PLGA-grafted HA (30:70) reacted for 120 min

2.6. XRD patterns

XRD analysis was performed to determine whether the crystallinity of HA changed after surface grafting with PLGA. The XRD patterns with different reaction time are shown in Figure 25(a). PLGA-grafted HA powders display similar patterns to that of HA. One difference is the peak height. When the reaction time increases, heights of the entire patterns slightly decrease. This indicates that in the sample of PLGA-grafted HA powders, other non-crystalline material like grafted PLGA exists besides HA.

For the detailed analysis, the XRD patterns of the non-grafted HA and PLGA-g-HA powders are presented in Figure 25(b); the average crystallite sizes (D) and crystalline fractions (X_c) are summarized in Table 7. HA exhibits four intense peaks at the diffraction angles of 25.9, 31.82, 32.1, and 32.82°, corresponding to the (002), (211), (112), and (300) planes of HA, respectively. PLGA-g-HA shows the same peaks, consistent with the crystalline nature of HA, even after surface grafting; this agrees with previously reported results (Murugan and Rao 2003, Wang, Dai et al. 2010). This suggests that surface grafting does not induce the formation of secondary phases in the HA crystalline lattice (Wang, Dai et al. 2010). However, the diffraction pattern also confirms that PLGA-g-HA has crystalline characteristics originating from HA, indicating that the PLGA polymer chains are successfully grafted onto the HA surfaces in the PLGA-g-HA particles. PLGA may exhibit a broad, low-intensity peak between 10 and 30°, as it is amorphous in nature (Kim and Park 2004, Ignjatović, Djurić et al. 2014), but it is clear that only a small amount of PLGA is grafted onto the HA surface in that the PLGA appears unclear in the XRD pattern. PLGA and HA are verified as homogeneous in distribution in the PLGA-g-HA particles because the total peak intensities of the PLGA-g-HA pattern were slightly lower than those of the non-grafted HA. The diffraction plane (002) relates to the overall average crystallite size D of HA particles (He and Huang 2007), so its peak is used to calculate D by using Scherrer's equation. As shown in Table 4, D and X_c show small decreases after surface grafting because of the effects of PLGA polymer chains, as previously reported (Rusu, Ng et al. 2005), but the intrinsic crystalline structure of HA is maintained in the PLGA-g-HA powder. In summary, the PLGA-g-HA powder seemed to form a new crystalline structure based on SEM observations; however, it is more plausible that the PLGA-g-HA particles are agglomerated by increased attraction between adjacent PLGA polymer chains by mechanisms such as H bonding or van der Waals forces. This agglomeration

may also affect the thermal and mechanical properties of the composite prepared by re-dispersion, as discussed later in Chapter 3.

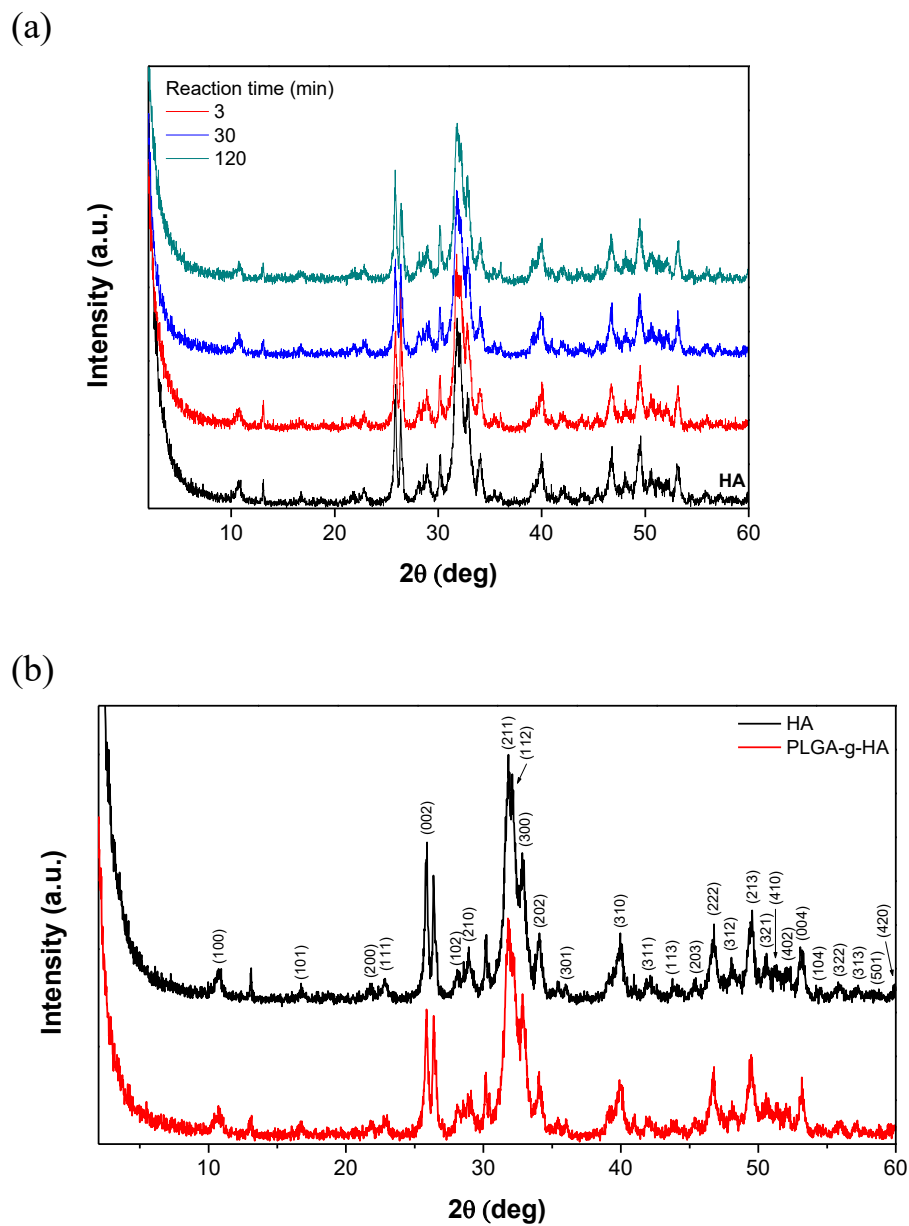


Figure 25. Powder XRD patterns of non-grafted HA and PLGA-grafted HA powders:

(a) Powder XRD patterns with different reaction time

(b) Peak comparison between HA and PLGA-g-HA

Table 7. Crystallite size and fraction crystallinity of non-grafted HA and PLGA-g-HA powders

	Bragg angle (°)	FWHM (°)	FWHM (rad)	<i>D</i> (nm)	<i>X_c</i>
non-grafted HA	25.848	0.291	0.00508	29.29	0.561
PLGA-g-HA	25.852	0.313	0.00547	27.19	0.450

3. Conclusion

The surface modification of HA was attempted to improve the biocomposites consisting of PLGA and HA. To find the optimal condition, the mixtures of PLGA:HA ratios of 10:90, 20:80, 30:70, and 50:50 were prepared and reacted for 3, 5, 10, 30, 60, and 120 min, respectively. PLGA-grafted HA powders as the second sediments and the first supernatants for GPC measurement were separated through the centrifugation and washing.

PLGA-grafted HA powders were characterized using TGA, GPC, FTIR, NMR, SEM, and XRD. TGA isothermal tests and temperature sweep tests of PLGA and HA confirm the thermal stability before thermal composition temperatures thus the concept of the grafted weight fraction was introduced to calculate how many PLGA polymer chains were grafted onto HA. The calculated grafted weight fractions generally increase as the reaction time increases and the ratio of PLGA increases except for the case of excessive PLGA. The optimal condition of grafting reaction was selected with the maximum grafted weight fraction of 10.032 wt%. This condition was named as “PLGA-g-HA” (PLGA:HA = 30:70 and 30 min reacted). The first supernatants were indirectly used to figure out the effect of the reaction on the molecular weights. GPC measurements lead to the reduction of the molecular weights and change of polydispersity indices, which supports the occurrence of the grafting reaction. Through FTIR analysis, it is confirmed that the surface grafting reaction between PLGA and HA occurs by esterification, as the spectra near 1720 cm^{-1} corresponding to C=O linkages changed. Likewise, solid-state ^1H NMR spectra displays the decreases at -0.10 ppm and 5.23 ppm corresponding to structural hydroxyl groups and surface-absorbed water molecules, respectively. The structural hydroxyl groups of 3.125% participated in the reaction as calculated using the reference peaks. SEM observation and XRD patterns additionally support the occurrence of the reaction by the morphological change of PLGA-grafted HA powders.

Chapter 3

Thermal, mechanical and viscoelastic properties of
PLGA/HA composites with different preparation methods

1. Experimental

1.1. Preparation of the PLGA/PLGA-g-HA composites

A mass of PLGA-g-HA was ground into powder and PLGA pellets were milled in a mortar, respectively. PLGA/PLGA-g-HA composite precursors were prepared through three different blending methods before injection molding. All composites were prepared such that the weight ratio of PLGA:PLGA-g-HA was 70:30. The first method was extrusion using a twin-screw compounding extruder BA-7 ($L/D = 40/7$) (Bautek, Republic of Korea). The temperatures of all four heating zones in the extruder were 170 °C. The screw speed was 100 rpm and its torque was 3.00 N·m. The extrudates were cut using a pelletizer. The second method was simply blending milled PLGA with PLGA-g-HA powders using a shaker at 200 rpm for 3 h. The third method was dispersing PLGA and PLGA-g-HA in chloroform by magnetic stirring at 50 °C for 6 h. The suspension was dried at 50 °C for 24 h to remove the residual chloroform and then cut into small pieces. After blending through these different methods, tensile test specimens and DMA specimens were prepared using an injection-molding machine (Bautek, Republic of Korea). Each specimen was blended by a 100-rpm rotor for 5 min under heating at 170 °C. The samples were named depending on the blending methods as PLGA/g-HA₁, PLGA/g-HA₂, PLGA/g-HA₃ for the first, second, and third method, respectively. As a control, a PLGA:HA mixture of 70:30 by weight was heat treated at 200 °C for 3 min.

1.2. Characterization of the PLGA/PLGA-g-HA composites

1.2.1. DSC

DSC analysis was performed using a DSC Q200 (TA Instruments, USA) apparatus with a refrigerator cooling system (RCS 90) to determine the glass transition (T_g), crystallization (T_c), and melting (T_m) temperatures of PLGA-g-HA. Samples of ~5 mg were loaded in Al pans with 50.0-mL/min high-purity N₂ used as the purge gas. The samples were first scanned from 30 to 200 °C at a heating rate of 10 °C/min to erase previous thermal history. After rapid quenching to -50 °C, the samples were scanned from -50 to 200 °C at a heating rate of 5 °C/min. The degree of crystallinity (X_c) was calculated using the following equation:

$$X_c (\%) = (\Delta H_m / \Delta H_f^0) \times 100$$

where ΔH_m is the enthalpy of fusion of the specimen and ΔH_f^0 is 93.7 J/g, which is the enthalpy of fusion for 100% crystalline PLA (Hong, Zhang et al. 2005).

1.2.2. Tensile testing

Dogbone-shaped tensile specimens were prepared according to ASTM D638 (Type V). Tensile testing was performed using an AllroundLine Z010 Universal Testing Machine (UTM) (Zwick, Germany) at a crosshead speed of 10 mm/min at RT. A 200-kN load cell with a pincer 8222 grip and extensometer was used for the test under the grip-to-grip separation of 20 mm and pre-loading of 1 N at a rate of 5 mm/min. At least five specimens were tested for each blending method and the tensile strength, modulus, and elongation were obtained by averaging data from five specimens.

1.2.3. DMA

Rectangular DMA specimens were prepared measuring 60 mm × 12 mm × 3 mm. DMA was performed using a DMA Q800 apparatus (TA Instruments, USA). The measurements were performed under the multi-frequency-strain mode at a fixed frequency of 1 Hz using a dual-cantilever clamp with a 35-mm span length and a purge fluid of 50-mL/min liquid N₂. The oscillating amplitude was 40 μm. The temperature scanning range was from 30 to 140 °C at the heating rate of 3 °C/min. The storage modulus, loss modulus, and damping factor ($\tan(\delta)$) were measured.

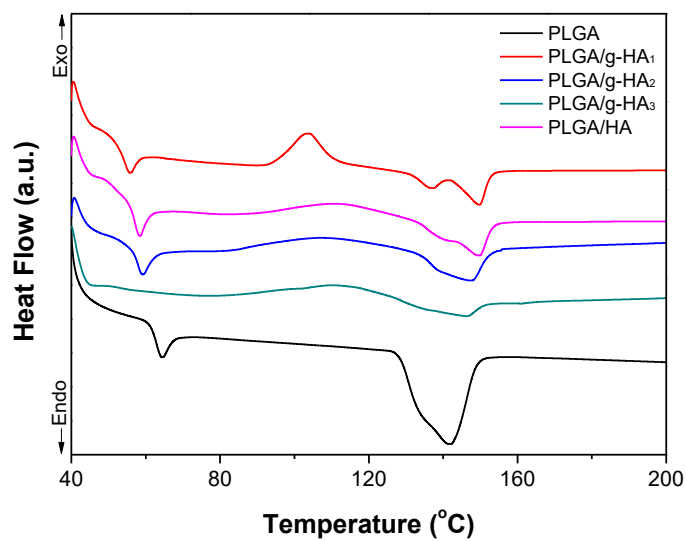
2. Results and Discussion

2.1. Thermal properties

DSC data of neat PLGA, PLGA/HA, and PLGA/PLGA-g-HA composites blended by different methods are shown in Figure 26 and Table 8; in details, such as T_g , T_c , T_m , and X_c for the first and second heating scan. In thermograms, the composites exhibit broad exothermic crystallization peaks and uncertain endothermic melting peaks because of their previous thermal histories. Therefore, the thermal properties, except for the T_g of samples and the T_m and ΔH_m of PLGA, were analyzed from the second heating scan. PLGA (L-lactide:glycolide = 82:18) is generally ~10% crystalline (Gilding and Reed 1979), but the X_c of PLGA found here is significantly higher. This may result from the partial crystallization of L-lactide units by the influence of the previous thermal history (or possibly other, uncertain reasons). To calculate the degree of crystallinity, the enthalpy of fusion of 100% crystalline PLA was used, because PLGA copolymers with 25–75% glycolide units are fully amorphous; for <25% glycolide units, there is too little glycolide to form crystalline regions, but L-lactide units could crystallize instead (Gilding and Reed 1979). Each T_g , T_c , and T_m in the first scan is lower than those in the second scan. Compared to neat PLGA, the composites show a greater decrease in T_g ; PLGA/g-HA₁ has the highest decrease. This means that the thermal stability of PLGA was relatively poor, possibly because of additional reactions of unreacted HA surface hydroxyl groups with adjacent PLGA. The PLGA polymer chains of PLGA/g-HA₁ were the most degraded by heat because of the extrusion molding process used for blending. Therefore, extrusion molding is inappropriate to create composites consisting of PLGA and non-grafted HA because the composites show low thermal stabilities. Meanwhile, PLGA shows no crystallization peak, but the composites clearly do in Figure 26. This can be explained by the nucleating ability of the HA fillers to crystallize PLGA polymer chains, which may contribute to the enhanced mechanical properties of the composites (He and Huang 2007). The T_g is decreased upon the addition of the HA or PLGA-g-HA, suggesting that the fillers affect the organization and orientation of PLGA polymer chain packing (Song, Ling et al. 2013). The fillers could affect chain mobility to reduce constriction in the amorphous regions of the polymer chains (Rahman, Afrin et al. 2014, Almasi, Ghanbarzadeh et al. 2015), thereby causing T_g to decrease. The T_m is increased upon the addition of the non-grafted HA or PLGA-

g-HA, suggesting stronger interactions between the PLGA matrix and filler. The composites display two melting transition peaks in the thermograms. The occurrence of double melting peaks is a common phenomenon for semi-crystalline polymers, resulting from the melt-reorganization of less ordered crystals (Wang, Song et al. 2017). Therefore, semi-crystalline regions of L-lactide units might be formed by the segmentation of PLGA polymer chains by reaction with HA, which also explains the non-zero X_c values of the composites with PLGA, despite PLGA's amorphous nature. Furthermore, all PLGA/PLGA-g-HA specimens, except for PLGA/g-HA₁, show higher T_g , T_c , T_m , and X_c values compared to PLGA/HA, indicating stronger physical linking and improved compatibility between the PLGA matrix and PLGA-g-HA. Among the PLGA/PLGA-g-HA specimens, PLGA/g-HA₁ was the lowest, PLGA/g-HA₂ median, and PLGA/g-HA₃ the highest in T_g , T_c , T_m , and X_c . The T_m of PLGA/g-HA₂ and PLGA/g-HA₃ are higher than that of neat PLGA. This indicates that, for PLGA/PLGA-g-HA, the thermal properties of composites differ significantly depending on the preparation methods; the re-dispersion of PLGA-g-HA enhances the physical miscibility and nucleating effects during composite preparation.

(a)



(b)

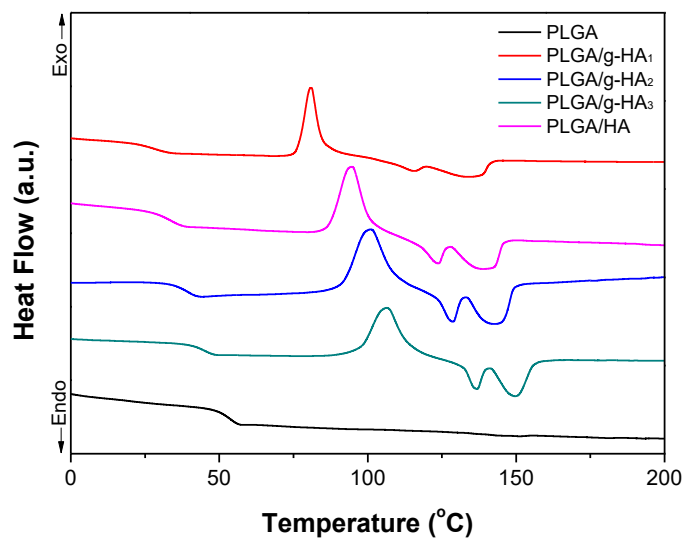


Figure 26. DSC thermograms of neat PLGA, PLGA/HA, and PLGA/PLGA-g-HA composites:

(a) First heating scan

(b) Second heating scan

Table 8. Thermal properties of neat PLGA, PLGA/HA and PLGA/PLGA-g-HA composites

		T_g (°C)	T_c (°C)	T_m (°C)	ΔH_m (J/g)	X_c (%)
First heating scan	PLGA	61.51	-	141.78	25.50	27.21
	PLGA/g-HA ₁	54.47	103.94	149.69	15.14	16.16
	PLGA/g-HA ₂	58.05	107.37	147.67	9.04	9.65
	PLGA/g-HA ₃	58.86	110.33	145.72	6.70	7.15
	PLGA/HA	57.30	111.64	149.73	9.31	9.94
Second heating scan	PLGA	53.51	-	-	-	-
	PLGA/g-HA ₁	28.35	80.97	134.14	12.09	12.90
	PLGA/g-HA ₂	39.36	100.93	142.92	13.80	14.73
	PLGA/g-HA ₃	45.56	106.40	149.58	15.09	16.10
	PLGA/HA	34.01	94.70	138.49	13.07	13.95

2.2. Mechanical properties

The representative stress–strain curves of neat PLGA, PLGA/HA, and PLGA/PLGA-g-HA composites are shown in Figure 27; their tensile strengths, elongations at break, and elastic moduli are shown in Figure 28. The stress–strain curves of PLGA and PLGA/HA are characteristic of ductile materials, but those of PLGA/PLGA-g-HA are characteristic of brittle materials. The neat PLGA exhibits the highest tensile strength and the highest elongation at break. For PLGA/HA, the introduction of HA deteriorates the mechanical properties of the PLGA matrix. However, the composite with HA is necessary for high biocompatibility, despite the decrease of mechanical properties. Compared to PLGA/HA, all PLGA/PLGA-g-HA specimens exhibit greater tensile strengths in Figure 28. Regardless of preparation method, PLGA-g-HA shows higher compatibility with the PLGA matrix than non-grafted HA does. This is because the PLGA polymer chains grafted on the HA surface penetrate the oriented alignment of PLGA matrix, therefore crystallizing and entangling with more matrix polymer chains throughout the matrix–filler interface. Among the PLGA/PLGA-g-HA specimens, PLGA/g-HA₃ has the highest tensile strength and PLGA/g-HA₁ the lowest. Therefore, the re-dispersion of filler enhances tensile strength because of the high degree of dispersion; however, extrusion molding deteriorates the tensile strength because of the thermal degradation of polymer chains and additional reactions with unreacted surface hydroxyl groups of HA. This agrees with the X_c measured by DSC. PLGA/g-HA₁ shows a lower T_g than the others, which suggests that the PLGA polymer chains grafted on the HA surfaces are shortened. This loosens the entanglement between PLGA matrix and filler, thus causing decreases in tensile strength. Furthermore, the change in X_c of the composites has the same tendency as the change in their tensile strengths. High tensile strength is clearly caused by the high X_c of PLGA/PLGA-g-HA. PLGA/HA exhibits higher elongation at break compared to all PLGA/PLGA-g-HA specimens. This means that PLGA/PLGA-g-HA gains enhanced tensile strength at the expense of ductility, while PLGA/HA maintains ductility even when blended with HA. Nevertheless, PLGA/PLGA-g-HA shows no plastic deformation region in Figure 27, meaning that these composites can respond to stress elastically to some extent. As shown in Figure 28, PLGA/PLGA-g-HA have slightly increased elastic moduli than neat PLGA and higher elastic moduli than PLGA/HA. The PLGA-g-HA filler negatively affects the strength of polymer matrix, but positively affects the stiffness of the composites. This may also be attributed to the entanglement between the grafted PLGA polymer chains and PLGA matrix in contrast with

the non-grafted HA. The elastic moduli of the composites show tendencies similar to those of their tensile strengths. In a previous study (Almasi, Ghanbarzadeh et al. 2015), this tendency was explained by three different mechanisms: surface compatibility and increased matrix–filler interactions, decreased free inter-chain spaces, and increased composite crystallinity. These three mechanisms can explain the results measured by DSC and mechanical testing.

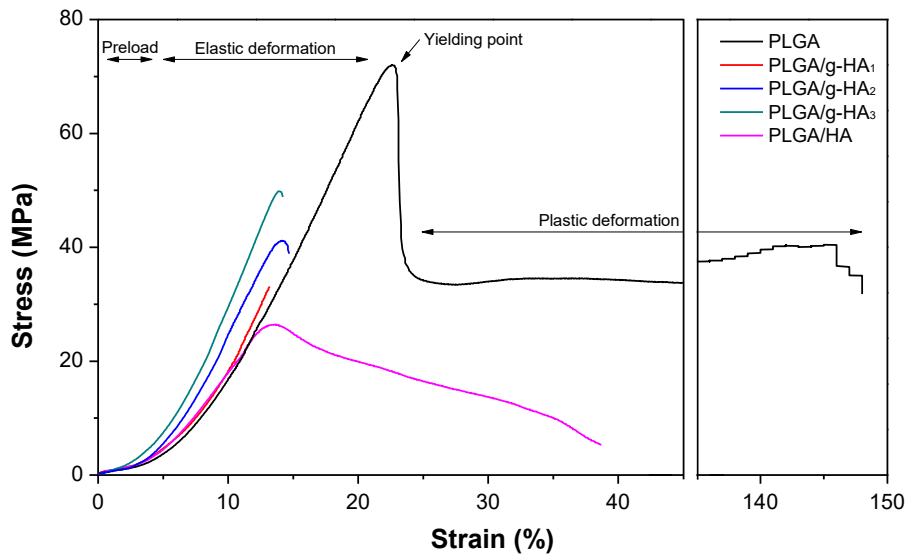


Figure 27. Representative stress-strain curves of neat PLGA, PLGA/HA, and PLGA/PLGA-g-HA composites

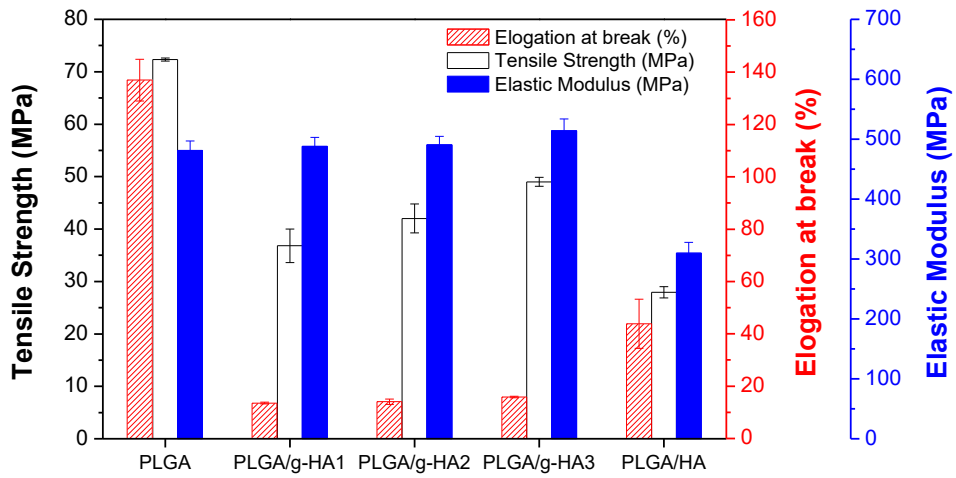


Figure 28. Tensile strengths, elongations at break, and elastic moduli of neat PLGA, PLGA/HA, and PLGA/PLGA-g-HA composites

2.3. Viscoelastic properties

DMA thermograms of neat PLGA, PLGA/HA, and PLGA/PLGA-g-HA composites are shown in Figure 29; detailed data, such as the storage moduli at 30, 60, 90, and 120 °C ($E'_{30^\circ\text{C}}$, $E'_{60^\circ\text{C}}$, $E'_{90^\circ\text{C}}$ and $E'_{120^\circ\text{C}}$, respectively), maximum $\tan \delta$ value ($(\tan \delta)_{\text{max}}$), glass transition temperature (T_g), effectiveness coefficient (C), and adhesion factor (A), are shown in Table 9. T_g is determined as the temperature at which the $\tan \delta$ is maximized. As shown in Figure 29(a) and Table 9, the $E'_{30^\circ\text{C}}$ of all composites are higher than that of PLGA, demonstrating the reinforcement effect of the fillers from matrix-filler interactions. This reinforcement is attributed to the effect of stiffness provided by the inorganic fillers to the polymer matrix, which indicates enhanced interfacial stress transfer within the composites (Akindoyo, Beg et al. 2017) and alignment with a more efficiently packed structure (Sonseca, Peponi et al. 2012). The storage moduli of all samples decrease sharply as the temperature increases. This glass transition is attributed to the increased chain mobility (Liu, Wang et al. 2014). In Figure 29(a), compared to PLGA, the composites display shorter plateau regions before T_g ; PLGA/HA has the shortest plateau region. This indicates the decreased thermal stability of the PLGA matrix, which may arise from the decreased chain length by grafting reactions with HA. All PLGA/PLGA-g-HA show longer plateau regions than PLGA/HA, indicating decreased thermal stability by additional reactions of unreacted hydroxyl groups on the surface of HA, as previously mentioned. As shown in Figure 29(b), the composites have higher loss modulus peaks than PLGA. This is attributed to the increase of chain segments and free volume of the PLGA matrix after the addition of HA, which inhibits stress relaxation within the composites (Romanzini, Lavoratti et al. 2013). In Figure 29(a) and (b), the storage and loss modulus decreased after T_g but increased slightly at ~ 90 °C, indicating the cold crystallization of the composites. After the increases in the modulus induced by crystallization, another decrease of the storage modulus occurs around 120–130 °C, indicating that the composites are softened at the onset of melting (Mofokeng, Luyt et al. 2012). The cold crystallization and softening are confirmed by DSC. As shown in Table 9, PLGA/PLGA-g-HA display higher T_g than PLGA/HA, and PLGA/g-HA₃ has even higher T_g than PLGA. This is caused by the agglomeration of PLGA-g-HA particles, as revealed by SEM micrographs. The agglomeration of filler restricts the mobility of polymer chains and thus increases the T_g (Liu, Wang et al. 2014). From PLGA/g-HA₃, the dispersion of filler within the polymer matrix effectively restricts the polymer chain mobility. The decrease in T_g of PLGA/g-HA₁ is ascribed to the low

thermal stability arising from thermal degradation during extrusion molding, as previously mentioned. The $\tan \delta$ values of PLGA and composites are presented in Figure 29(c), with $(\tan \delta)_{\max}$ summarized in Table 9. The $\tan \delta$ is an effective indicator of interfacial adhesion between the polymer matrix and filler; better adhesion corresponds to lower $\tan \delta$ values because of the decreased polymer chain mobility (Krishna and Kanny 2016). The improved interfacial adhesion is related to the enhanced stress transfer within the composites, and causes the enhancement in mechanical properties (Akindoyo, Beg et al. 2017). Therefore, the composites show improved interfacial adhesion in terms of $(\tan \delta)_{\max}$. Despite having the lowest $(\tan \delta)_{\max}$, however, PLGA/HA shows poor tensile strength and elastic modulus as seen in Figure 28. This contradiction can be explained by the high content of unreacted HA hydroxyl groups in PLGA/HA; therefore, additional reactions with HA shorten the chain length of the PLGA matrix and promote decreases in storage modulus, which indicates adhesion without sufficient entanglement.

For the further analysis, the effectiveness coefficient (C) and the adhesion factor (A) were introduced. C is defined as:

$$C = \frac{E'_g/E'_r \text{ (composite)}}{E'_g/E'_r \text{ (resin)}}$$

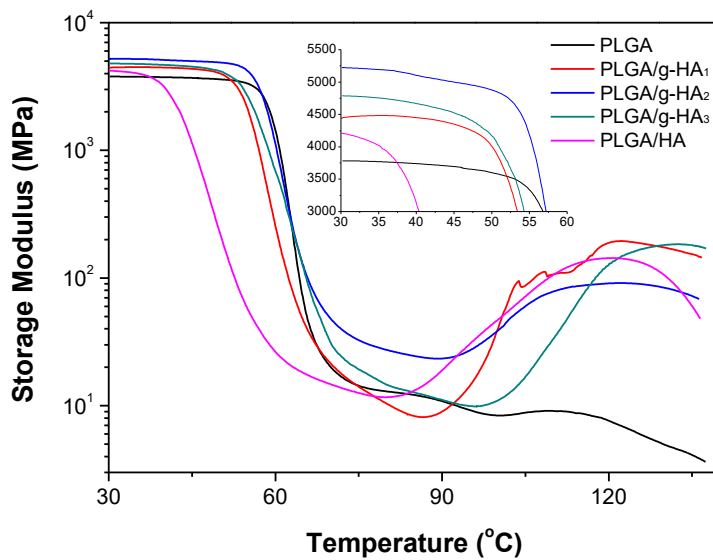
where E'_g is the storage modulus in the glassy state region (at 30 °C), and E'_r is the storage modulus in the rubbery state region (at 75 °C). It is reported that higher C means lower effectiveness (Romanzini, Lavoratti et al. 2013). PLGA/g-HA₂ and PLGA/g-HA₃ have low C , confirming that PLGA/PLGA-g-HA is more effective in transferring stress within the polymer matrix compared to PLGA and PLGA/HA. A is defined as:

$$A = \frac{1 - \tan \delta_c}{1 - V_f \tan \delta_p} - 1$$

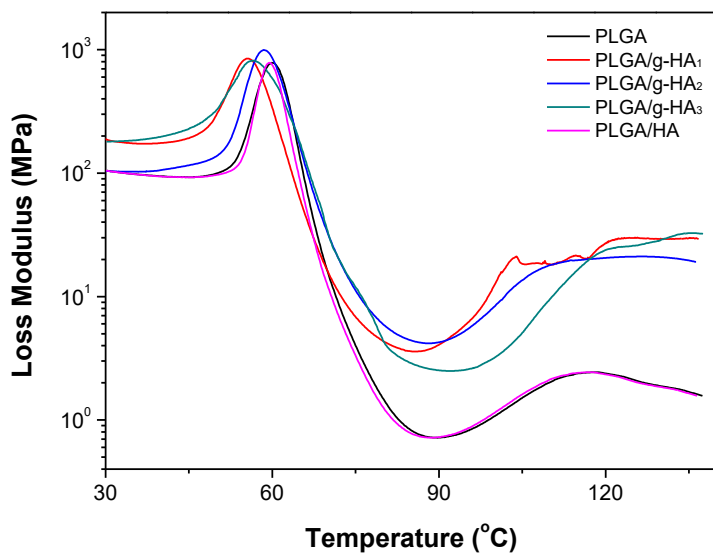
where $\tan \delta_c$ is the $\tan \delta$ of the composite, $\tan \delta_p$ is the $\tan \delta$ of the pure polymer (at 30 °C), and V_f is the volume fraction of the filler; here, the volume fraction is replaced with the weight fraction. It is reported that lower A corresponds to better interfacial adhesion (Correa, Razzino et al. 2007). PLGA/g-HA₂ and PLGA/g-HA₃ have low A values, confirming the strong adherence of PLGA-g-HA with the PLGA matrix at the interface. Meanwhile, PLGA/g-HA₂ has lower C and A values than PLGA/g-HA₃ has. Without re-dispersion, the PLGA-g-HA agglomerates are easily formed, as discussed in Chapter 2; this reduces the apparent volume fraction of the polymer matrix, as if more fillers were loaded (Song and Youn 2005). Therefore,

the stiffness of filler itself has greater influence on the storage moduli of poorly dispersed composites, leading to lower C and A values.

(a)



(b)



(c)

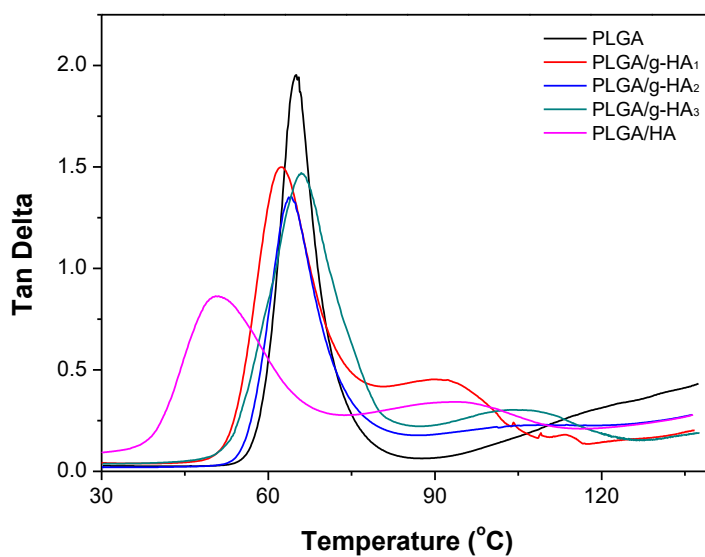


Figure 29. DMA thermograms of neat PLGA, PLGA/HA, and PLGA/PLGA-g-HA composites:

- (a) Storage modulus
- (b) Loss modulus
- (c) Tan delta

Table 9. Viscoelastic properties of neat PLGA, PLGA/HA and PLGA/PLGA-g-HA composites

	$E'_{30^{\circ}\text{C}}$ (MPa)	$E'_{60^{\circ}\text{C}}$ (MPa)	$E'_{90^{\circ}\text{C}}$ (MPa)	$E'_{120^{\circ}\text{C}}$ (MPa)	(tan δ) _{max}	T_g ($^{\circ}\text{C}$)	C	A
PLGA	3738.27	1375.85	10.83	7.61	1.95	65.07	1.000	0.000
PLGA/g-HA ₁	4438.53	257.30	9.01	188.51	1.50	62.33	1.197	1.186
PLGA/g-HA ₂	5224.13	1113.27	23.41	90.81	1.35	64.01	0.608	0.021
PLGA/g-HA ₃	4788.22	667.60	11.07	127.54	1.47	65.95	0.936	0.928
PLGA/HA	4212.04	26.47	18.92	143.12	0.86	51.02	1.509	3.761

3. Conclusion

On the basis of the analysis on the surface grafting reaction, the PLGA:HA ratio of 30:70 reacted for 30 min (named as “PLGA-g-HA”) was chosen for the composites among PLGA-grafted HA. The precursors containing PLGA and PLGA-g-HA with the ratio of 70:30 were prepared by three different preparation methods: Extrusion molding, simple blending, and re-dispersion. Eventually, the composites containing PLGA and PLGA-g-HA were prepared using an injection-molding machine.

PLGA/PLGA-g-HA composites were characterized using DSC, UTM, and DMA. PLGA-g-HA particles had influences on the thermal, mechanical and viscoelastic properties of the composites according to preparation methods. PLGA/PLGA-g-HA composites exhibit enhanced mechanical properties compared to PLGA/HA composite. Furthermore, the composites prepared by simple blending (PLGA/g-HA₂) and re-dispersion (PLGA/g-HA₃) showed improved storage modulus and improved tensile strength, respectively, while the composite prepared by extrusion molding (PLGA/g-HA₁) showed lowered tensile strength and storage modulus. Through DSC analysis, it is also found that each composite displays different thermal properties such as the glass transition temperature, the melting temperature, and the degree of crystallinity. Therefore, heat, dispersion, and interfacial adhesion between PLGA and HA are identified as the critical factors which determine mechanical properties of the composites. Our results indicate that preparation methods have a strong influence on properties of the composites and they could be manipulated for specific contexts after the surface grafting reaction and preparation methods are fully understood.

References

- Aissa, A., et al. (2007). "Covalent modification of calcium hydroxyapatite surface by grafting phenyl phosphonate moieties." Journal of Solid State Chemistry **180**(8): 2273-2278.
- Akindoyo, J. O., et al. (2017). "Effects of surface modification on dispersion, mechanical, thermal and dynamic mechanical properties of injection molded PLA-hydroxyapatite composites." Composites Part A: Applied Science and Manufacturing.
- Almasi, H., et al. (2015). "Novel nanocomposites based on fatty acid modified cellulose nanofibers/poly (lactic acid): Morphological and physical properties." Food Packaging and Shelf Life **5**: 21-31.
- Ashok, M., et al. (2003). "Crystallization of hydroxyapatite at physiological temperature." Materials Letters **57**(13): 2066-2070.
- Azimi, B., et al. (2014). "Poly (lactide-co-glycolide) Fiber: An Overview." Journal of Engineered Fabrics & Fibers (JEFF) **9**(1).
- Barber, F. A., et al. (1995). "Preliminary results of an absorbable interference screw." Arthroscopy: The Journal of Arthroscopic & Related Surgery **11**(5): 537-548.
- Borum, L. and O. Wilson (2003). "Surface modification of hydroxyapatite. Part II. Silica." Biomaterials **24**(21): 3681-3688.
- Chlopek, J., et al. (2009). "FTIR and NMR study of poly (lactide-co-glycolide) and hydroxyapatite implant degradation under in vivo conditions." Polymer Degradation and Stability **94**(9): 1479-1485.
- Choi, H. W., et al. (2006). "Surface modification of hydroxyapatite nanocrystals by grafting polymers containing phosphonic acid groups." Journal of colloid and interface science **304**(1): 277-281.
- Correa, C., et al. (2007). "Role of maleated coupling agents on the interface adhesion of polypropylene—wood composites." Journal of Thermoplastic Composite Materials **20**(3): 323-339.
- Cui, Y., et al. (2009). "The nanocomposite scaffold of poly (lactide-co-glycolide) and hydroxyapatite surface-grafted with L-lactic acid oligomer for bone repair." Acta biomaterialia **5**(7): 2680-2692.
- Cummins, C. A., et al. (2003). "Rotator cuff repair with bioabsorbable screws: an in vivo and ex vivo investigation." Arthroscopy: The Journal of Arthroscopic & Related Surgery **19**(3): 239-248.
- Degirmenbasi, N., et al. (2006). "Biocomposites of nanohydroxyapatite with collagen and poly (vinyl alcohol)." Colloids and Surfaces B: Biointerfaces **48**(1): 42-49.

- Erbetta, C. D. A. C., et al. (2012). "Synthesis and characterization of poly (D, L-lactide-co-glycolide) copolymer." Journal of Biomaterials and Nanobiotechnology **3**(02): 208.
- Gilding, D. and A. Reed (1979). "Biodegradable polymers for use in surgery— polyglycolic/poly (actic acid) homo-and copolymers: 1." Polymer **20**(12): 1459-1464.
- He, Q. J. and Z. L. Huang (2007). "Controlled growth and kinetics of porous hydroxyapatite spheres by a template-directed method." Journal of crystal growth **300**(2): 460-466.
- Hong, Z., et al. (2004). "Grafting polymerization of L-lactide on the surface of hydroxyapatite nano-crystals." Polymer **45**(19): 6699-6706.
- Hong, Z., et al. (2005). "Nano-composite of poly (L-lactide) and surface grafted hydroxyapatite: mechanical properties and biocompatibility." Biomaterials **26**(32): 6296-6304.
- Hu, Y., et al. (2014). "Facile fabrication of poly (l-lactic acid)-grafted hydroxyapatite/poly (lactic-co-glycolic acid) scaffolds by pickering high internal phase emulsion templates." ACS applied materials & interfaces **6**(19): 17166-17175.
- Ignjatović, N., et al. (2014). "Investigating an organ-targeting platform based on hydroxyapatite nanoparticles using a novel in situ method of radioactive 125 Iodine labeling." Materials Science and Engineering: C **43**: 439-446.
- Ito, K., et al. (1985). "Reactivity of poly (ethylene oxide) macromonomers in radical copolymerization." Polymer journal **17**(7): 827.
- Jose, M. V., et al. (2009). "Aligned PLGA/HA nanofibrous nanocomposite scaffolds for bone tissue engineering." Acta biomaterialia **5**(1): 305-315.
- Kim, H. K. and T. G. Park (2004). "Comparative study on sustained release of human growth hormone from semi-crystalline poly (L-lactic acid) and amorphous poly (D, L-lactic-co-glycolic acid) microspheres: morphological effect on protein release." Journal of Controlled Release **98**(1): 115-125.
- Krishna, K. V. and K. Kanny (2016). "The effect of treatment on kenaf fiber using green approach and their reinforced epoxy composites." Composites Part B: Engineering **104**: 111-117.
- Lee, H. J., et al. (2006). "Modification of hydroxyapatite nanosurfaces for enhanced colloidal stability and improved interfacial adhesion in nanocomposites." Chemistry of materials **18**(21): 5111-5118.
- Lee, S., et al. (2005). "Biomechanical comparison of bioabsorbable sutureless screw anchor versus suture anchor fixation for rotator cuff repair." Arthroscopy: The Journal of

- Arthroscopic & Related Surgery **21**(1): 43-47.
- Li, J., et al. (2008). "Effect of surface modified hydroxyapatite on the tensile property improvement of HA/PLA composite." Applied Surface Science **255**(2): 494-497.
- Liu, Q., et al. (1998). "Polyacids as bonding agents in hydroxyapatite polyester-ether (Polyactive™ 30/70) composites." Journal of Materials Science: Materials in Medicine **9**(1): 23-30.
- Liu, Q., et al. (1998). "Surface modification of nano-apatite by grafting organic polymer." Biomaterials **19**(11-12): 1067-1072.
- Liu, X., et al. (2014). "Effects of inorganic fillers on the thermal and mechanical properties of poly (lactic acid)." International journal of polymer science **2014**.
- Mingalyov, P., et al. (2011). "Solid-state NMR spectroscopic study of the structure of grafted layers of phosphonic acid ester-modified hydroxyapatite." Colloid Journal **73**(1): 83-87.
- Misra, D. (1985). "Adsorption of zirconyl salts and their acids on hydroxyapatite: use of the salts as coupling agents to dental polymer composites." Journal of dental research **64**(12): 1405-1408.
- Mofokeng, J. P., et al. (2012). "Comparison of injection moulded, natural fibre-reinforced composites with PP and PLA as matrices." Journal of Thermoplastic Composite Materials **25**(8): 927-948.
- Murugan, R. and K. P. Rao (2003). "Graft polymerization of glycidylmethacrylate onto coralline hydroxyapatite." Journal of Biomaterials Science, Polymer Edition **14**(5): 457-468.
- Nair, L. S. and C. T. Laurencin (2007). "Biodegradable polymers as biomaterials." Progress in polymer science **32**(8): 762-798.
- Palacio, J., et al. (2011). "Effect of the molecular weight on the physicochemical properties of poly (lactic acid) nanoparticles and on the amount of ovalbumin adsorption." Journal of the Brazilian Chemical Society **22**(12): 2304-2311.
- Panda, R., et al. (2003). "FTIR, XRD, SEM and solid state NMR investigations of carbonate-containing hydroxyapatite nano-particles synthesized by hydroxide-gel technique." Journal of Physics and Chemistry of Solids **64**(2): 193-199.
- Pawaskar, A. C., et al. (2015). "Magnetic resonance appearance of bioabsorbable anchor screws for double row arthroscopic rotator cuff repairs." Indian journal of orthopaedics **49**(2): 164.

- Petricca, S. E., et al. (2006). "Chemical synthesis of poly (lactic-co-glycolic acid)/hydroxyapatite composites for orthopaedic applications." Acta biomaterialia **2**(3): 277-286.
- Phua, K., et al. (2011). Degradable Polymers. Comprehensive biomaterials. P. Ducheyne, Elsevier. **1**: 381-415.
- Qiu, X., et al. (2005). "Hydroxyapatite surface modified by L-lactic acid and its subsequent grafting polymerization of L-lactide." Biomacromolecules **6**(3): 1193-1199.
- Rahman, M. M., et al. (2014). "Preparation and characterization of jute cellulose crystals-reinforced poly (l-lactic acid) biocomposite for biomedical applications." International Journal of Chemical Engineering **2014**.
- Ren, T., et al. (2005). "The bone formation in vitro and mandibular defect repair using PLGA porous scaffolds." Journal of biomedical materials research Part A **74**(4): 562-569.
- Reyes-Gasga, J., et al. (2013). "XRD and FTIR crystallinity indices in sound human tooth enamel and synthetic hydroxyapatite." Materials Science and Engineering: C **33**(8): 4568-4574.
- Romanzini, D., et al. (2013). "Influence of fiber content on the mechanical and dynamic mechanical properties of glass/ramie polymer composites." Materials & Design **47**: 9-15.
- Rusu, V. M., et al. (2005). "Size-controlled hydroxyapatite nanoparticles as self-organized organic-inorganic composite materials." Biomaterials **26**(26): 5414-5426.
- Song, X., et al. (2013). "Electrospun hydroxyapatite grafted poly (L-lactide)/poly (lactic-co-glycolic acid) nanofibers for guided bone regeneration membrane." Composites science and technology **79**: 8-14.
- Song, Y. S. and J. R. Youn (2005). "Influence of dispersion states of carbon nanotubes on physical properties of epoxy nanocomposites." Carbon **43**(7): 1378-1385.
- Sonseca, A., et al. (2012). "Electrospinning of biodegradable polylactide/hydroxyapatite nanofibers: study on the morphology, crystallinity structure and thermal stability." Polymer Degradation and Stability **97**(10): 2052-2059.
- Wang, X., et al. (2002). "Development of biomimetic nano-hydroxyapatite/poly (hexamethylene adipamide) composites." Biomaterials **23**(24): 4787-4791.
- Wang, Y., et al. (2010). "Improved mechanical properties of hydroxyapatite/poly (ϵ -caprolactone) scaffolds by surface modification of hydroxyapatite." Applied Surface Science **256**(20): 6107-6112.

- Wang, Y., et al. (2017). "Preparation of Desirable Porous Cell Structure Polylactide/Wood Flour Composite Foams Assisted by Chain Extender." Materials **10**(9): 999.
- Wilson, E. E., et al. (2006). "Three structural roles for water in bone observed by solid-state NMR." Biophysical journal **90**(10): 3722-3731.
- Wong, K., et al. (2009). "Mechanical properties and in vitro response of strontium-containing hydroxyapatite/polyetheretherketone composites." Biomaterials **30**(23): 3810-3817.
- Xiao, Y., et al. (2007). "Preparation of nano-HA/PLA composite by modified-PLA for controlling the growth of HA crystals." Materials Letters **61**(1): 59-62.
- Xu, Z.-K., et al. (2009). Surface engineering of polymer membranes, Springer Science & Business Media.
- Yesinowski, J. P. and H. Eckert (1987). "Hydrogen environments in calcium phosphates: proton MAS NMR at high spinning speeds." Journal of the American Chemical Society **109**(21): 6274-6282.
- Zhang, P., et al. (2009). "In vivo mineralization and osteogenesis of nanocomposite scaffold of poly (lactide-co-glycolide) and hydroxyapatite surface-grafted with poly (L-lactide)." Biomaterials **30**(1): 58-70.

초 록

본 논문에서는, 하이드록시아파타이트 (Hydroxyapatite, HA) 표면에 위치하는 하이드록실 (hydroxyl) 작용기에 직접적으로 Poly(lactide-*co*-glycolide) (PLGA) 공중합체의 고분자 체인을 그래프팅하여, PLGA와 PLGA가 그래프팅된 하이드록시아파타이트 (PLGA-g-HA) 간의 복합재료의 계면 접착력에 하이드록시아파타이트의 표면 개질이 미치는 영향과 그에 따른 물성 변화에 대해 관찰하고자 하였다.

적외선 분광분석 (FTIR) 과 핵자기공명 분광분석 (NMR) 을 통해 하이드록시아파타이트 표면에서의 에스터 (ester) 결합이 형성됨을 확인하였다. 열중량 분석 (TGA) 을 통해 표면에 그래프팅된 고분자의 양은 10.032 wt% 임을 확인하였다. 고체상 수소 NMR 스펙트럼 결과를 통해 그래프팅 이후 하이드록시아파타이트 표면의 하이드록실 작용기의 양이 3.125% 감소했음을 확인하였다. 겔 투과 크로마토그래피 (GPC) 분석을 통해 그래프팅에 따른 분자량 감소를 확인하였다. X선 회절 분석 (XRD) 패턴과 주사 전자 현미경 (SEM) 관찰을 통해 그래프팅이 성공적으로 일어났음을 추가적으로 확인하였다.

하이드록시아파타이트 표면에 PLGA를 그래프팅한 후 세 가지 방법으로 PLGA/PLGA-g-HA 복합재료를 제조하였다: 압출 가공, 단순 블렌딩, 재분산 후 사출 가공. 제조된 복합재료의 열적, 기계적, 점탄성적 물성을 각각 시차 주사 열량계 (DSC), 인장강도 테스트, 동적 점탄성 분석기 (DMA) 를 통해 분석하였다. 세 가지 분석 결과에 따르면, 복합재료의 제조방법이 최종적인 복합재료의 물성에 중요한 영향을 미친다는 결과를 확인하였다.

키워드: Poly(lactide-*co*-glycolide) (PLGA) 공중합체; 하이드록시아파타이트 (Hydroxyapatite, HA); 표면 그래프팅 반응; 복합재료; 제조 방법

학번: 2017-25623